HHS Public Access

Author manuscript

Cancer Res. Author manuscript; available in PMC 2022 July 29.

Published in final edited form as:

Cancer Res. 2022 May 16; 82(10): 1872–1889. doi:10.1158/0008-5472.CAN-21-2106.

M^{6}A RNA Methylation Regulates Histone Ubiquitination to Support Cancer Growth and Progression

Pooja Yadav[1,2], **Panneerdoss Subbarayalu**[1,2], **Daisy Medina**[1,2], **Saif Nirzhor**[1,2], **Santosh Timilsina**[1,2], **Subapriya Rajamanickam**[1,3], **Vijay K. Eedunuri**[1], **Yogesh Gupta**[1,4], **Siyuan Zheng**[1], **Nourhan Abdelfattah**[5], **Yufei Huang**[6], **Ratna Vadlamudi**[7], **Robert Hromas**[8], **Paul Meltzer**[9], **Peter Houghton**[1,3], **Yidong Chen**[1,10], **Manjeet K. Rao**[1,2]

[1]Greehey Children's Cancer Research Institute, University of Texas Health Science Center at San Antonio, San Antonio, Texas.

[2]Department of Cell Systems and Anatomy, University of Texas Health Science Center at San Antonio, San Antonio, Texas.

[3]Department of Molecular Medicine, University of Texas Health Science Center at San Antonio, San Antonio, Texas.

[4]Department of Biochemistry, University of Texas Health Science Center at San Antonio, San Antonio, Texas.

[5]Houston Methodist Research Institute, Houston, Texas.

[6]Department of Electrical and Computer Engineering, University of Texas at San Antonio, San Antonio, Texas.

[7]Department of Obstetrics and Gynecology, University of Texas Health Science Center at San Antonio, San Antonio, Texas.

[8]Department of Medicine, University of Texas Health Science Center at San Antonio, San Antonio, Texas.

[9]Center for Cancer Research, National Cancer Institute, Bethesda, Maryland.

[10]Department of Epidemiology and Biostatistics, University of Texas Health Science Center at San Antonio, San Antonio, Texas.

Abstract

Corresponding Author: Manjeet K. Rao, Greehey Children's Cancer Research Institute, University of Texas Health Science Center, 8403 Floyd Curl Drive, San Antonio, TX 78229. Phone: 210–562–9119, raom@uthscsa.edu.

Authors' Contributions

P. Yadav: Formal analysis, validation, investigation, visualization, methodology, writing–original draft. **P. Subbarayalu:** Formal analysis, validation, investigation, visualization, methodology. **D. Medina:** Validation, investigation, visualization, methodology. **S. Nirzhor:** Validation, investigation, visualization, methodology. **S. Timilsina:** Validation, investigation, visualization, methodology. **S. Rajamanickam:** Formal analysis, validation, investigation, visualization, methodology. **V.K. Eedunuri:** Formal analysis, validation, methodology. **Y. Gupta:** Validation, methodology. **S. Zheng:** Software. **N. Abdelfattah:** Formal analysis. **Y. Huang:** Software. **R. Vadlamudi:** Formal analysis, validation, methodology. **R. Hromas:** Formal analysis, methodology. **P. Meltzer:** Formal analysis. **P. Houghton:** Formal analysis, methodology. **Y. Chen:** Data curation, software, formal analysis, validation, visualization. **M.K. Rao:** Conceptualization, resources, data curation, formal analysis, supervision, funding acquisition, validation, investigation, visualization, methodology, writing–original draft, writing–review and editing.

Note: Supplementary data for this article are available at Cancer Research Online (http://cancerres.aacrjournals.org/).

Osteosarcoma is the most common malignancy of the bone, yet the survival for patients with osteosarcoma is virtually unchanged over the past 30 years. This is principally because development of new therapies is hampered by a lack of recurrent mutations that can be targeted in osteosarcoma. Here, we report that epigenetic changes via mRNA methylation holds great promise to better understand the mechanisms of osteosarcoma growth and to develop targeted therapeutics. In patients with osteosarcoma, the RNA demethylase *ALKBH5* was amplified and higher expression correlated with copy-number changes. ALKBH5 was critical for promoting osteosarcoma growth and metastasis, yet it was dispensable for normal cell survival. Methyl RNA immunoprecipitation sequencing analysis and functional studies showed that ALKBH5 mediates its protumorigenic function by regulating m^6A levels of histone deubiquitinase USP22 and the ubiquitin ligase RNF40. ALKBH5-mediated m^6A deficiency in osteosarcoma led to increased expression of USP22 and RNF40 that resulted in inhibition of histone H2A monoubiquitination and induction of key protumorigenic genes, consequently driving unchecked cell-cycle progression, incessant replication, and DNA repair. RNF40, which is historically known to ubiquitinate H2B, inhibited H2A ubiquitination in cancer by interacting with and affecting the stability of DDB1-CUL4–based ubiquitin E3 ligase complex. Taken together, this study directly links increased activity of ALKBH5 with dysregulation of USP22/RNF40 and histone ubiquitination in cancers. More broadly, these results suggest that m^6A RNA methylation works in concert with other epigenetic mechanisms to control cancer growth.

Significance: RNA demethylase ALKBH5 upregulates USP22 and RNF40 to inhibit histone H2A ubiquitination and induces expression of key replication and DNA repair–associated genes, driving osteosarcoma progression.

Introduction

Osteosarcoma is the most common bone malignancy in children and adolescents, with a second peak in incidence in those over the age of 50 (1). Most osteosarcomas (80%–90%) are high-grade tumors with poorly understood etiology. Unfortunately, the survival for patients with metastatic or relapsed osteosarcoma has remained virtually unchanged over the past 30 years, with an overall 5-year survival rate of about 20% (2). This rate has not improved due to lack of effective alternatives to chemotherapy. Moreover, surviving patients have highly compromised quality of life due to debilitating side effects associated with high doses of chemotherapy received early in life. In the last three decades, virtually no drug has been approved for treating osteosarcoma. This is in part because osteosarcoma has highly disorganized genome and no recurrent mutation/s that can be targeted have been identified. Those facts underline the importance of identifying new targets and mechanisms that can help better understand the osteosarcoma pathogenesis.

RNA modifications represent one such possibility. Of the >150 known RNA modifications, N^6-methyadenosine (m^6A) is the most abundant mark in mRNA. M^6A is regulated by a dynamic and reversible process involving RNA methyltransferase complex proteins (writers) and demethylases (erasers; ref. 3). Methyltransferase like 3 (METTL3), METTL14, Wilms' tumor 1 associated protein (WTAP), and other accessory proteins constitute the writer complex (4), while AlkB Homolog 5 (ALKBH5) and Fat mass and obesity-associated protein (FTO) are RNA demethylases that act as erasers of m^6A marks (5, 6). In addition

to writers and erasers, the fate of transcripts harboring m^6A is decided by the "reader" proteins that recognize the m^6A mark (7). It is becoming clear that m^6A regulates different aspects of RNA metabolism, from mRNA processing to decay and translation of specific set of transcripts (8). M^6A methylation also plays a critical role in different biological processes, including development, stem cell fate decision (9), the circadian clock (10), neuronal differentiation, and immunity (11). Emerging evidence suggests that in addition to normal physiologic events, m^6A proteins may be important in pathologic conditions, including cancer. For example, METTL3 promotes growth of acute myeloid leukemia and osteosarcoma (12–14). In addition, ALKBH5 supports the breast cancer stem cell phenotype (15) and maintain tumorigenicity of glioblastoma stem-like cells. The role of ALKBH5 in osteosarcoma is not clear as one study suggested that ALKBH5 may have a tumor suppressor function in osteosarcoma, while another report showed an oncogenic function for ALKBH5 in osteosarcoma (16, 17). A more thorough study is needed to clarify the function and mechanism of action of ALKBH5 in cancer in general and osteosarcoma in particular.

In this study, we show that the RNA demethylase *ALKBH5* is amplified in large cohorts of osteosarcoma and plays a critical role in promoting osteosarcoma growth and progression. ALKBH5 mediates its protumorigenic function by inducing the stability of histone deubiquitinase ubiquitin specific peptidase 22 (USP22) and ubiquitin ligase RING finger protein 40 (RNF40) in a RNA methylation-dependent manner. USP22 is a subunit of the SAGA transcriptional coactivator complex that alters chromatin structure and induces epigenetic changes by removing the monoubiquitin moiety from histones H2A and H2B (18). RNF40 cooperates with the ubiquitin ligase RNF20 and the E2 ubiquitin conjugative enzyme RAD6 to monoubiquitinate H2B (19). USP22 is overexpressed in multiple cancers including osteosarcoma and its expression is associated with tumor aggressiveness and poor prognosis (20). USP22 may have a causal role in tumor progression by activating the transcription and/or protein stability of transcription factors and cell cycle–associated genes, including c-myc, cyclin B1 (21), and cyclin D1 (22). In addition, recent studies have demonstrated that USP22 promotes resistance to chemotherapy by promoting DNA strand break repair (23). Similar to USP22, RNF40 has a tumor-promoting role in many cancers including breast, prostate, and hepatocellular carcinoma. Yet in some cancers, it is reported to act as a tumor suppressor (24–26).

We show that ALKBH5 supports osteosarcoma growth by promoting cell-cycle progression, replication, and DNA damage repair. In particular, our results reveal that silencing of ALKBH5 increases m^6A levels and consequently destabilizes USP22 and RNF40, resulting in reduced expression of several genes associated with cell cycle, replication and DNA damage repair in osteosarcoma cells. Our further analysis revealed that increased activity/amplification of ALKBH5 leads to induction of USP22/RNF40-dependent protumorigenic event in osteosarcoma.

Our study, for the first time, shows that m^6A RNA methylation is a critical regulator of histone ubiquitination events in cancers in general and osteosarcoma in particular. Notably, we show that RNF40 inhibits H2A ubiquitination by binding and affecting the stability of damaged DNA binding protein 1 (DDB1)–CUL4A ubiquitin ligase complex that targets H2A monoubiquitination at the site of DNA damage.

Materials and Methods

Cell culture

The human cancer cell lines 143B, U2OS, and Saos2, and the control cell line human fetal osteoblasts (hFOB) were all purchased from the ATCC and cultured in standard growth medium according to their guidelines. IMR-90 cells (lung fibroblasts) were kindly provided by Dr. Gregory Aune's laboratory. The osteosarcoma cell line OS-17 came from a patient-derived xenograft of osteosarcoma and was a gift from Dr. Peter Houghton's laboratory. OS-17 cells were grown in RPMI supplemented with 10% FBS and 1% penicillin/streptomycin. All cell lines except hFOB were maintained in a humidified incubator at 37°C and 5% CO_2. hFOB cells were grown at 34°C in a humidified incubator with 5% CO_2.

Migration and colony formation assays

Osteosarcoma cells were transfected with either scrambled siRNA or ALKBH5 siRNAs (Sigma-Aldrich) for 48 hours. Transfection was carried out using the RNAiMAX Reagent (Thermo Fisher Scientific) according to the manufacturer's protocol. Cells were then harvested and subjected to long-term clonogenic and migration assays (27). For migration assays, 24-well transwell plates (8-μm pore size, Corning) were used. For rescue experiments, 143B cells (1.1×10^5) or U2OS (1.8×10^5) cells were seeded in 6-well plates. Cells were cotransfected with control, USP22-, or RNF40-overexpressing plasmid along with either scrambled siRNA or ALKBH5 siRNAs using Lipofectamine 2000 (Thermo Fisher) according to the manufacturer's protocol. After 48 hours, cells were subjected to clonogenic assays as described above. Plasmids were purchased from GenScript (RNF40-pcDNA3.1-C-(k) DYK ORF clone OHu08721D and USP22_OHu25420D).

Cell viability and proliferation assays

Osteosarcoma cells were seeded in 96-well plates at 2.5×10^3 cells per well and transfected with scrambled or ALKBH5/USP22/RNF 40siRNA using RNAiMAX Reagent (Thermo Fisher) according to the manufacturer's protocol. Cell viability was assessed using CellTiter-Glo (Promega) or AlamarBlue (Thermo Fisher). Cell proliferation was assessed using IncuCyte proliferation assays for live-cell analysis.

Cell-cycle analysis and apoptosis assays

Osteosarcoma cells were seeded in 6-well plates and transfected with either scrambled siRNA or ALKBH5 siRNAs (Sigma-Aldrich). After 48 hours, cells were stained with propidium iodide and Annexin V–fluorescein isothiocyanate (FITC) to analyze apoptosis. For cell-cycle analyses, cells were first fixed using 70% ethanol for 24 hours followed by propidium iodide staining. Cells were analyzed in FACSCanto II or LSR II cytometers and data were analyzed using FlowJo software (version 10.2).

Stable cells

Lentiviral vector-expressing nontargeting pLKO.1 control shRNA and shRNA targeting ALKBH5 (28) were a gift from Dr. Suyun Huang (MD Anderson Cancer Center, Houston,

TX). For lentiviral production, 293T cells were transfected with lentiviral vectors along with the packaging vectors psPAX2 and pMD2G (Addgene). For stable cell line generation, osteosarcoma cells were transduced with viral particles with 8 μg/mL polybrene (Sigma-Aldrich). After 48 hours, 1 μg/mL puromycin was added for selection of stable cells over four days.

Animal and tumor xenograft studies

All animal experimental procedures were approved by the Institutional Animal Care and Use Committee at the University of Texas Health San Antonio (San Antonio, TX). For tumor xenograft studies, 143B cells stably expressing scrambled shRNA or ALKBH5 shRNA (1×10^6) were injected subcutaneously into the flanks of 4-week-old athymic nude mice (n = 8/group; purchased from Envigo, Inc.). For orthotopic xenograft and experimental metastasis models, 143B cells stably expressing GFP-luc and scrambled shRNA or ALKBH5 shRNA (1×10^6) were injected into tibia or via tail vein, respectively, of 4-week-old athymic nude mice. Equal numbers of male and female mice were used. Tumor volumes and body weight were measured twice a week. Tumor volumes for subcutaneous injection model were measured using caliper and for intratibial and experimental metastasis models using Xenogen *in vivo* imaging system. At the end time point, mice were euthanized, and the tumors isolated and processed for molecular studies. Tumor volume was calculated using the formula $0.5236L_1 (L_2)^2$, where L_1 is the long axis and L_2 is the short axis of the tumor. For tumor xenograft studies using siRNA, 143B cells transfected with scrambled or ALKBH5 siRNAs (1×10^6) were injected subcutaneously into the flanks of 4-week-old athymic nude mice (purchased from Envigo, Inc.). Tumor volume was calculated as described above.

RNA and protein

Total RNA extracted from osteosarcoma cell lines were subjected to qRT-PCR. Protein samples for Western blot were prepared from total cell lysate. Cancer cell lines were transfected with scrambled siRNA or ALKBH5 siRNA (Sigma-Aldrich) for 48 or 72 hours before they were subjected to qRT-PCR or Western blot analysis, as described previously (42). Chromatin immunoprecipitation (ChIP)-qPCR was done using an EZ-Magna ChIP A/G Chromatin Immunoprecipitation Kit according to the manufacturer's instructions. Primers used in this study are listed in Supplementary Table S4. Antibodies against ALKBH5 (#HPA007196) and β-actin (#A3854) were purchased from Sigma-Aldrich. Antibodies against USP22 (#ab195289, 1:1,000) were purchased from Abcam Inc. Antibodies against P27/KIP1 (#2552), Ubiquityl-Histone H2A (Lys119) (D27C4) (#8240), Histone H2B (D2H6) (#12364), Ubiquityl-Histone H2B (Lys120) (#5546), WEE1 (#4936S), CDK2 (#2546), RNF40 (#12187S), and Cyclin B1 (#4135) were purchased from Cell Signaling Technology. Antibodies against MCM2 (#sc-56322), MCM4 (#sc-48407), and CDC25A (#sc-7389) were purchased from Santa Cruz Biotechnology. Actinomycin D (catalog no. A1410) was purchased from Sigma-Aldrich.

RNA sequencing

For whole-genome transcriptome profiling, four libraries were generated from total RNA from scrambled siRNA– and ALKBH5 siRNA–transfected 143B cells, using a TruSeq Stranded mRNA Library Preparation kit according to the manufacturer's protocol (Illumina

Inc.). Samples were sequenced on the Illumina HiSeq 2000 platform (Illumina Inc.) using the 50 base-pair single-read (50SR) sequencing module. Sequence reads were mapped to the University of California, Santa Cruz (UCSC) genome build hg19 using TopHat2 aligner (v2.0.6) with default parameters for stranded RNA. Gene expression was measured by HTSeq, and differential analyses were performed using DESeq. Upregulated and downregulated genes were determined by the following criteria: (i) absolute $\log_2$ fold change >1 (29), average RPKM (reads per kilobase per million mapped reads) >1, and (iii) multiple test adjusted (Benjamini–Hochberg) *P* value <0.05. The differentially expressed genes are provided in Supplementary Tables S1 and S5. Using the differential expression fold change, we also performed Gene Set Enrichment Analysis (GSEA), using the stand-alone package from the Broad Institute (v4.0.3). We preselected 123 pathways/gene sets from mSigDB (v7.1) that included various terms related to DNA repair, DNA duplication, E2F, PRC1/2, and histone ubiquitination. Raw data have been deposited in Gene Expression Omnibus (GSE154530). Raw data for U2OS RNA-seq has been submitted to GEO.

For methyl RNA immunoprecipitation sequencing (Me-RIP-seq) analyses, total RNA was isolated from scrambled and ALKBH5-siRNA–transfected 143B cells using TRIzol (Thermo 15596018) followed by mRNA isolation using a Dynabeast Direct Kit (Life Tech 61012). Two micrograms of polyadenylated mRNA was diluted to 100 μL in water and fragmented to 100 to 200 nucleotides using Bioruptor (Diagenode). Five microliters of RNA was used for input preparation. Two micrograms of fragmented mRNA was used for immunoprecipitation (18) using rabbit anti-m^6A antibody (Synaptic Systems #202003) in immunoprecipitation (IP) buffer (10 mmol/L Tris pH 7.4, 150 mmol/L NaCl, 0.1% NP-40) for 2 hours at 4°C. After incubation, samples were added to Protein A beads and incubated for 2 more hours at 4°C with rotation. After washing, samples were eluted using elution buffer containing m^6A nucleoside and elute was concentrated using a Zymo RCC-5 column. The resultant final product was used for RNA-sequencing (RNA-seq). 0.1 μg of fragmented mRNA was used as input control for RNA sequencing. Two additional m^6A antibodies used were MABE1006 (Millipore Sigma) and ABE572 (Millipore Sigma).

Me-RIP-seq and data preprocessing

Precipitated RNA was resuspended in H_2O and used for library generation with the TruSeq stranded Total RNA Library Prep kit (Illumina). Equal amounts of barcoded samples were pooled together and submitted for cluster generation on an Illumina cBot Cluster Station and then sequencing on an Illumina HiSeq 3000 system using the 50SR sequencing module, according to the manufacturer's instructions. Similar to RNA-seq, the obtained sequence reads were first mapped to the UCSC human genome build hg19 using the TopHat2 aligner (v2.0.6). Total reads and mapped reads are listed in Supplementary Table S5. We further processed alignment data (BAMs) to convert to TDF format for visualization using SAMTools. For any pairs of samples (meRIP vs. Input), we applied MeTPeak program (30) to identify m6A enrichment sites, and used Guitar tools (31) to generate peak distributions, and using MEME-ChIP program for m^6A motif enrichment analysis.

Global and differential m^{6}A methylation determination from me-RIP-seq

Differential m^{6}A methylation analyses from Me-RIP-seq data were carried out using methods similar to those in our earlier publications (32). Specifically, we used an improved version of our earlier software package, exomePeak (33), with the MeTDiff (30) for methylation peak calling and differential peak identification. MeTDiff modeled the reads variation in the meRIP data using an effective likelihood ratio test to evaluate differential methylation significance, with better robustness and higher sensitivity and specificity. The program generates methylation fold change of the percentages of methylated fragments for a specific mRNA locus, where a positive value indicates high (hyper-) m^{6}A methylation in the treated condition compared with the untreated condition, whereas a negative value indicates lower (hypo-) methylation, along with their statistical significance (*P* values) and multiple-test adjusted *P* values. Significant differential peaks were selected with adjusted *P* value < 0.05 (Supplementary Table S2). The output of MeTDiff was then fed into the Guitar software (31), which plots the distribution of the differential m^{6}A sites in transcripts.

RNA methylation quantification

m^{6}A RNA methylation was detected using dot blot assays as previously described (34). Briefly, 500 ng of total RNA isolated from scrambled or ALKBH5 siRNA cells was blotted on an Amersham Hybond-N+ membrane (GE Healthcare, catalog number: RPN203B) and crosslinked using Stratalinker 2400 UV Crosslinker (Stratalinker). The membrane was blocked using non-fat milk and incubated with anti-m^{6}A antibody (ABE572, Millipore Sigma) overnight followed by incubation with anti-rabbit IgG-HRP (Santa Cruz Biotechnology, catalog number: sc-2004) secondary antibody for 1 hour at room temperature. Amersham Hyperfilm ECL (GE Healthcare, catalog number: 28906835) film was used for data acquisition.

RIP

ALKBH5 RIP was carried out using a Magna RIP RNA-Binding Protein Immunoprecipitation Kit (Sigma, 17–700) according to the manufacturer's protocol. 3.5 μg of anti-ALKBH5 antibody (Sigma, HPA007196) was used for each reaction, with the same amount of IgG used as a control.

Homologous recombination and nonhomologous end joining assays

I-SceI–based DNA repair assays were performed using U2OS cells with stably integrated DR-GFP(HR) or EJ5-GFP constructs obtained from Drs. Maria Jasin and Jeremy Stark. Cells were seeded in 12-well plates in antibiotic-free media and transfected with siRNAs using RNAiMAX Reagent (Thermo Fisher). After 24 hours, cells were transfected with I-SceI expression vector or empty vector as controls. Cells were harvested after 72 hours and GFP-positive cells were evaluated by flow cytometry on a BD FACSCANTO II flow cytometer. Data were analyzed using FlowJo software (version 10.2).

DNA synthesis assays

DNA synthesis assays were carried out using a Click-iT EdU Alexa Fluor 647 Flow Cytometry Assay Kit according to the manufacturer's protocol. Briefly, cells were

labeled with nucleoside analogue EdU (5-ethynyl-2′-deoxyuridine) at 10 μmol/L final concentration. Cells were fixed, permeabilized, and a Click-iT Reaction was carried out to detect incorporated EdU using flow cytometry. For bromodeoxyuridine (BrdU) incorporation, cells were incubated with 10 μmol/L BrdU for 30 minutes to pulse-label the cells. Cells were washed, harvested, and fixed with ice-cold ethanol. Cells were washed and incubated with 2N HCl/0.5% Triton X-100 for denaturation and neutralized with 0.1 mol/L sodium borate (Na_2B4O_7, pH 8.5). Samples were incubated with anti-BrdU (Becton Dickinson) antibody for 30 minutes at room temperature. After washing, cells were incubated with Alexa 488–labeled goat anti-mouse antibody. Cells were washed and resuspended in PBS containing 5 μg/mL propidium iodide for labeling DNA. Samples were analyzed by flow cytometry.

Immunofluorescence and IHC

Immunofluorescence assays were done in osteosarcoma cells fixed with 4% paraformaldehyde as described previously (27). IHC was carried out by the UTHSA Histology & Immunohistochemistry Core Laboratory using an anti-ALKBH5 (Sigma, HPA007196) antibody on tissue microarray cores from US Biomax, Inc. (osteosarcoma tissue array-OS804c and bone tissue- BO244f).

Statistical analyses

GraphPad software was used for statistical analysis. All values and error bars in graphs represent means ± SEM, unless noted otherwise. Respective *n* values are indicated in the figure legends. *P* values were determined by two-tailed Student *t* tests and ANOVA as required for appropriate statistical testing.

Data availability statement

All data supporting the conclusion in this article are present in the paper and/or the Supplementary Materials. Some data generated in this study are publicly available in Gene Expression Omnibus (GEO) at GSE154530. Additional data related to this article may be requested from the corresponding author.

Results

ALKBH5 is amplified and highly expressed in osteosarcoma and promotes its growth and progression

To begin to understand the role of m^6A regulators in cancers, we analyzed the expression of m^6A writers and erasers in patient-derived xenografts (PDX) from different pediatric and adult cancers using PDX for childhood cancer therapeutics database (PCAT; ref. 35). Of all the m^6A regulators, ALKBH5 showed the highest expression in osteosarcoma compared with other cancer types (Fig. 1A; Supplementary Fig. S1A–S1C). IHC analysis on tissue microarrays also showed markedly higher expression of ALKBH5 in 40 osteosarcoma samples compared with 11 normal bone samples (Supplementary Fig. S1D). In accordance with those results, comparative genomic hybridization and RNA-sequencing analysis of 97 primary osteosarcoma samples revealed that in comparison to METTL3, METTL14, or FTO, ALKBH5 is highly amplified in osteosarcoma (>26%–40%), and its expression is

highly correlated with copy-number changes (Fig. 1B; Supplementary Fig. S1E). Next, we determined whether there is a negative correlation between levels of m^6A and expression of ALKBH5 in osteosarcoma. Colorimetric analysis showed that m^6A level is lower in osteosarcoma cell lines compared with the normal fetal osteoblast (hFOB) and fibroblast (IMR90) cells, while expression of ALKBH5 is comparatively higher in osteosarcoma cell lines compared with hFOB and IMR90 as revealed by Western blot analysis (Supplementary Fig. S1F and S1G).

To examine the functional significance of ALKBH5 overexpression, we silenced its expression in multiple osteosarcoma cell lines using two different small interfering RNAs (siRNA). ALKBH5 was significantly decreased at the RNA and protein levels compared with scrambled siRNA (Supplementary Fig. S2A–S2C). ALKBH5 knockdown resulted in significantly increased levels of overall m^6A levels, whereas ALKBH5 overexpression decreased m^6A levels in osteosarcoma cells (Supplementary Fig. S2D). Next, we assessed the effect of ALKBH5 depletion on osteosarcoma cells. Silencing of ALKBH5 resulted in reduced proliferation, short-term viability, and clonogenic growth of osteosarcoma cells (143B, U2OS, and Saos2; Fig. 1C–E, G–L; Supplementary Fig. S2E–S2G). ALKBH5 silencing also significantly diminished the migratory ability of osteosarcoma cells, as assessed by transwell migration assays (Supplementary Fig. S2H and S2I). Similar to ALKBH5 silencing using siRNAs, stable knockdown of ALKBH5 using shRNA significantly reduced the levels of ALKBH5 and consequently decreased short- and long-term cell viability and migration of osteosarcoma cells (Supplementary Fig. S3A–S3G). Next, we determined whether demethylase activity of ALKBH5 is essential for its protumorigenic activity in osteosarcoma. ALKBH5 overexpression rescued, while ALKBH5 catalytic mutant could not rescue the effect of ALKBH5 silencing on clonogenicity and migration of osteosarcoma cells (Supplementary Fig. S4A and S4B). To determine the specificity of ALKBH5 silencing, we examined the levels of related mammalian AlkB homologs. ALKBH5 silencing did not significantly affect the level of ALKBH3, neither did stable depletion of ALKBH5 led to compensatory upregulation of another m6A demethylase FTO (Supplementary Fig. S4C and S4D).

To confirm our *in vitro* results, we performed multiple tumor xenograft studies. Stable silencing of ALKBH5 led to significantly reduced osteosarcoma growth in a mouse tumor xenograft model (Fig. 1M; Supplementary Fig. S4E and S4F). Next, we used a second tumor xenograft model using a siRNA against ALKBH5 that targets a region different than shRNA used for the stable knockdown of ALKBH5. Similar to stable knockdown model, ALKBH5 siRNA transfectant showed significantly smaller tumor compared with scrambled transfectant (Supplementary Fig. S4G and S4H). To further validate these results, we used an intratibial orthotopic xenograft model. Intratibial transplantation of 143B cells stably expressing ALKBH5 shRNA resulted in markedly smaller tumor compared with scrambled control (Fig. 1N; Supplementary Fig. S4I). To investigate whether ALKBH5 may also promote tumor metastasis, we used the experimental lung metastasis model, which recapitulates extravasation, seeding, and growth of metastatic process. Scrambled and ALKBH5 shRNA stably transfected 143B-GFP-luc cells were injected via tail vein. ALKBH5 shRNA transfectant tumors had no or very small lung lesions, while scrambled transfectant had macrometastasis in the lungs (Fig. 1O). Next, we determined whether

ALKBH5 knockdown affected normal cells. ALKBH5 knockdown using two different siRNAs resulted in significantly reduced ALKBH5 levels in both hFOB and IMR-90 (Supplementary Figs. S2C and S4J) and had no effect on growth and viability of hFOB and IMR-90 fibroblasts (Fig. 1F; Supplementary Fig. S4K). This result is consistent with the observation that ALKBH5 knockout mice were viable and anatomically normal except for impaired fertility (6). Taken together, these results suggest that ALKBH5 may be an important promoter of osteosarcoma growth and metastasis but is dispensable for normal cell proliferation.

ALKBH5 regulates expression of DNA replication, cell-cycle, and DNA damage repair genes

To understand how ALKBH5 may promote osteosarcoma growth and progression, we performed RNA sequencing (RNA-seq) analysis on ALKBH5 silenced 143B and U2OS cells (Fig. 2A; Supplementary Table S1; Supplementary Fig. S5A). Gene ontology and pathway analyses of differentially expressed genes revealed that cell-cycle, DNA replication, and DNA damage repair were among the highly enriched biological processes downregulated in ALKBH5 KD cells (Fig. 2B; Supplementary Fig. S5B–S5D). Consistent with the RNA-seq results, DNA replication–associated genes (*CDC45*, *MCM2*, *RRM1*, *CDC7*, and *PCNA*); cell-cycle progression genes (*E2F1* and cyclin-dependent kinases); and DNA repair genes (*RAD51* and *BRCA1*) had significantly reduced expression in ALKBH5 knockdown 143B and U2OS osteosarcoma cells compared with scrambled siRNA–transfected cells (Fig. 2C and D; Supplementary Fig. S5E and S5F).

The decreased expression of cell cycle–associated genes in ALKBH5 KD osteosarcoma cells prompted us to ask whether ALKBH5 may promote cell-cycle progression to support tumor growth. ALKBH5 depletion led to G_0–G_1 arrest in 143B and OS-17 and S–G_2 phase arrest cells in U2OS cells (Fig. 2E; Supplementary Fig. S5G). Although we do not completely understand the reason for S–G_2 arrest in U2OS cells, presence of wild-type retinoblastoma protein (Rb) in U2OS cells may be one of the reasons. Supporting that, DNA-damaging agents are shown to inhibit S-phase progression in $Rb^{+/+}$ but not in $Rb^{-/-}$ cells (36). It is possible that ALKBH5 knockdown–induced DNA damage leads to S-phase arrest in U2OS cells. Nevertheless, supporting the induction of cell-cycle arrest after ALKBH5 KD, expression of the cyclin-dependent kinases inhibitor protein $p27^{Kip1}$ and Wee1 increased (Fig. 2D; Supplementary Fig. S5F and S5H), whereas expression of the cell cycle–promoting genes was decreased in both 143B and U2OS cells (Fig 2C and D; Supplementary Fig. S5E, S5F, and S5H). However, ALKBH5 KD had no effect on cell-cycle progression in control hFOB cells (Fig 2E).

When we assessed whether ALKBH5 promotes DNA replication by measuring thymidine analogue 5-ethynyl-2′-deoxyuridine (32) incorporation, we found fewer EdU-positive cells in ALKBH5-silenced osteosarcoma cells compared with scrambled siRNA–transfected cells (Supplementary Fig. S6A). Further supporting this finding, pulse labeling with EdU or BrdU revealed significantly fewer replicating cells that incorporated thymidine analogues in ALKBH5-silenced osteosarcoma cells compared with scrambled siRNA–transfected U2OS cells (Fig. 2F; Supplementary Fig. S6B). This change was not due to decreased numbers of

cells in S-phase, because ALKBH5 KD in U2OS cells increased the proportion of S-phase cells (Supplementary Fig. S5G).

ALKBH5 depletion induces replication stress and impairs DNA damage repair

As ALKBH5 KD induced cell-cycle arrest and reduced the expression of DNA replication machinery, we wondered whether ALKBH5 depletion induces replication stress and consequently increases DNA damage. To address that, we performed DNA fiber analysis, which measures DNA replication at a single molecule resolution. We pulse-labeled scrambled and ALKBH5 siRNA–treated osteosarcoma cells sequentially with IdU and CldU and incubated them with IdU and CldU primary antibodies. Immunofluorescence analyses showed shorter DNA fiber lengths, reflecting slowed overall fork progression in ALKBH5 KD compared with scrambled siRNA–transfected cells (Supplementary Fig. S6C).

Next, we asked whether induced replication stress causes DNA damage in ALKBH5-silenced osteosarcoma cells. ALKBH5 KD increased levels of the DNA damage marker γH2AX without exposure to any exogenous DNA-damaging agents (Fig. 3A). Replication stress leads to CHK1 activation by ATR-dependent phosphorylation (Ser345) and subsequent phosphorylation of multiple target proteins that leads to cell-cycle arrest. Consistent with that finding, ALKBH5 silencing resulted in checkpoint activation, as revealed by increased CHK1 phosphorylation (Ser345) and decreased expression of its downstream target CDC25A (Fig. 3B; Supplementary Fig. S5H). To address whether increased DNA damage and replication stress resulted in apoptotic death, we performed Annexin V staining. Flow cytometry analyses showed increased apoptotic death in ALKBH5-silenced osteosarcoma cells compared with scrambled siRNA–transfected osteosarcoma cells (Fig. 3C; Supplementary Fig. S6D).

Because ALKBH5 silencing led to increased DNA damage and apoptosis, we reasoned that ALKBH5 depletion may impair DNA repair in osteosarcoma cells. We induced DNA damage in scrambled siRNA and ALKBH5 siRNA–transfected osteosarcoma cells by exposing them to ionizing radiation, and testing repair 24 hours later by measuring two markers of DNA double-strand breaks (DSB), γH2AX, and 53BP1 foci by flow cytometry and immunofluorescence, respectively. ALKBH5-silenced osteosarcoma cells had higher levels of γH2AX and increased numbers of 53BP1 foci (Fig. 3D and E; Supplementary Fig. S6E). Similar to siRNA, stable ALKBH5 KD cells also showed increased γH2AX foci when treated with or without ionizing radiation (Supplementary Fig. S7A and S7B). Because ALKBH family proteins are shown to be important regulators of alkylation-dependent DNA damage, we asked whether DNA alkylating agent may induce the expression of ALKBH5. Indeed, 5-fluorouracil treatment induced the expression of ALKBH5 in osteosarcoma cells (Supplementary Fig. S7C). Next, we determined the effect of ALKBH5 silencing on DNA damage response in normal cells. Similar to cell cycle, DNA repair processes do not seem to be altered in normal cells as γH2AX did not show any significant difference between ALKBH5-silenced and scrambled treated IMR90 or HEK293 cells (Supplementary Fig. S7D). These results suggest that ALKBH5 plays a critical role in DNA damage response and that damaged DNA may not be efficiently repaired in ALKBH5-silenced osteosarcoma cells.

Subsequently, our GSEA of RNA-seq data showed significant downregulation of DNA repair pathways, including DSB repair, in ALKBH5-silenced osteosarcoma cells (Fig. 3F). Because DSBs are primarily repaired by homologous recombination (HR) and nonhomologous end joining (NHEJ) repair mechanisms, we examined the effects of ALKBH5 KD on these repair pathways by performing I-SceI–based functional DNA repair assays. ALKBH5 depletion significantly reduced both HR and NHEJ-mediated DNA repair efficiency of U2OS cells (Fig. 3G and H). Overall, these results suggest that ALKBH5 promotes osteosarcoma cell growth and proliferation by supporting DNA replication, cell-cycle progression, and DNA damage repair.

Transcriptome-wide Me-RIP-seq identifies histone deubiquitinating protein USP22 as a ALKBH5 target

We sought to identify target mRNAs demethylated by ALKBH5 by performing me-RIP using a m^6A antibody followed by deep sequencing (MeRIP-seq) in scrambled siRNA and ALKBH5 KD 143B osteosarcoma cells. Using our MeTDiff algorithm (30), we identified 12,760 and 9,927 common and 2,378 and 7,636 unique m^6A peaks in scrambled and ALKBH5-silenced cells, respectively (Fig. 4A). Most m^6A enriched peaks were located in coding sequences followed by 3′UTR (Fig. 4B). Because ALKBH5 is an m^6A eraser, we considered genes with enriched m^6A peaks (Hyper m^6A) in ALKBH5-silenced osteosarcoma cells to be potentially regulated by ALKBH5-mediated m^6A demethylation.

When we combined our RNA-seq results with me-RIP-seq data, we identified 721 hypermethylated m^6A peaks whose mRNA transcripts were significantly downregulated (443, termed as hyper-down) or upregulated (278, hyper-up) in ALKBH5 KD cells compared with scrambled siRNA–treated cells ($P < 0.005$ and fold change ≥ 2; Fig. 4C). Among the 721 hyper m^6A peaks, 61.4% were associated with downregulated mRNA expression in ALKBH5 KD cells, whereas only 30.6% of hypo-m^6A peaks were downregulated in ALKBH5-KD cells (Fig. 4C; Supplementary Table S2). Notably, hypo-m^6A peaks were enriched in both 5′UTR and 3′UTR, while hyper-m^6A peaks were enriched mainly near the stop codon (Fig. 4D). These results indicate that most of ALKBH5's potential targets with increased m^6A have reduced expression in ALKBH5-depleted osteosarcoma cells.

We next focused on cell cycle- and DNA repair–associated genes, because ALKBH5 silencing in osteosarcoma cells reduced expression of those genes and consequently cell-cycle arrest and inhibition of DNA repair. Surprisingly, many of those cell cycle- and DNA repair–associated genes showed no significant differences in m^6A levels/peaks between ALKBH5-silenced and scrambled siRNA–transfected osteosarcoma cells.

Interestingly, USP22, which can regulate cell-cycle progression and DNA damage repair-associated gene expression by its deubiquitination activity (18, 23, 37), was the top hyper-m^6A down gene in ALKBH5-silenced osteosarcoma cells (Fig. 4C and E; hyper-m^6A is shown as differential peak fold change: FC = total m^6A value/expression of USP22 in ALKBH5 KD vs. scrambled siRNA). We further confirmed USP22 as an ALKBH5 demethylation target by performing me-RIP-seq using two additional m^6A antibodies (Supplementary Fig. S8A). Supporting that, a more quantitative me-RIP-qPCR analysis on

tumor tissues from ALKBH5 KD group and ALKBH5-silenced osteosarcoma cells showed significantly increased m^6A levels and decreased expression of USP22 compared with scrambled group (Supplementary Fig. S8B and S8C). Inspection of the 3′UTR of USP22 revealed that enriched m^6A peaks overlapped with m^6A-binding motifs (RRACH; Fig. 4E). ALKBH5 silencing led to significantly reduced expression of USP22 in 143B, U2OS, and OS-17 osteosarcoma cell lines (Fig. 4F; Supplementary Fig. S8D–S8G). Conversely, ALKBH5 overexpression increased USP22 expression in osteosarcoma cells (Fig. 4G; Supplementary Fig. S8H).

Previous studies showed that m^6A-modified mRNA transcripts exhibit reduced stability (9, 38, 39). Because ALKBH5 KD increased m^6A levels and significantly decreased USP22 mRNA steady-state levels, we performed mRNA stability analyses in scrambled siRNA and ALKBH5-silenced osteosarcoma cells. 143B and U2OS cells were treated with actinomycin D (to inhibit *de novo* transcription) for varying periods followed by qRT-PCR. ALKBH5 KD significantly reduced *USP22* mRNA stability compared with scrambled siRNA–treated cells (Supplementary Fig. S8I–S8J).

To further examine m^6A-dependent regulation of USP22, we silenced m^6A RNA methyltransferase METTL3 in ALKBH5 KD 143B cells and examined USP22 expression. Supporting the regulation of USP22 by m^6A modification, knockdown of the methyltransferase METTL3 increased USP22 expression in ALKBH5-silenced 143B cells (Fig. 4H; Supplementary Fig. S9A). Taken together, our data suggests that USP22 is highly sensitive to changes in m^6A levels and that ALKBH5 induces USP22 expression by maintaining an undermethylated state as increased methylation promotes accelerated decay of USP22 transcript in ALKBH5-depleted cells.

ALKBH5 regulates H2A K119 monoubiquitination via USP22 and RNF40

USP22 deubiquitinates both histones H2A (lysine 119) and H2B (lysine 120; ref. 40). Because ALKBH5 KD reduced USP22 expression, we wondered whether changes in ALKBH5 levels or activity affects H2A and H2B monoubiquitylation levels. We focused on monoubiquitinated form as monoubiquitinated H2A(H2Aub) and H2B (H2Bub) are the dominant form of ubiquitinated histones. Moreover, monoubiquitinated H2A and H2B have well-established roles in regulating transcription of target genes as H2Aub is predominantly associated with transcriptional repression, while H2Bub is mostly associated with transcriptionally active genes (41). On the other hand, polyubiquitination of H2A is required for specific DNA repair events or targets histones for proteasomal-mediated degradation (41). Our results revealed that the H2A monoubiquitination was increased at the lysine 119 residue (H2Aub) in ALKBH5 KD osteosarcoma cells, whereas ALKBH5 overexpression led to decreased H2Aub levels (Fig. 4F and G; Supplementary Fig. S9B–S9F). Consistent with that, H2Aub levels were significantly increased in ALKBH5 knockdown tumors compared with control (Supplementary Fig. S9G and S9H). There was no change in total H2A level observed (Supplementary Fig. S9I). The H2Aub increase in ALKBH5-silenced cells was not due to increased levels of writer proteins such as RING1/RNF2 (Supplementary Fig. S9J). We also tested the expression of USP3, USP16, and USP21 that are known to remove H2Aub (41). Our results showed that expression of USP3,

USP16 and USP21 did not show any significant change in ALKBH5 KD cells compared with scrambled siRNA–transfected osteosarcoma cells (Supplementary Fig. S9J).

To our surprise, we did not see consistent changes in H2B mono-ubiquitination (H2Bub) or total H2B levels after ALKBH5 KD or overexpression of ALKBH5 (Fig. 4F and G; Supplementary Fig. S9K). This could be due to altered expression of the H2BK120 monoubiquitination writer proteins RNF20/RNF40. Our me-RIP-seq data showed that RNF40 (but not RNF20) was hypermethylated (Fig. 5A; hyper-m^{6}A is shown as differential peak fold change: FC = total m^{6}A value/expression level of the RNF40 in ALKBH5KD vs. scrambled siRNA). These findings were further confirmed by me-RIP-seq analysis using two additional m^{6}A antibodies (Supplementary Fig. S10A). Consistent with these results, qPCR and Western blot analyses showed that ALKBH5 KD decreased RNF40 expression in osteosarcoma cells (Fig. 5B; Supplementary Fig. S10B–S10D). Conversely, overexpression of ALKBH5 led to increased RNF40 expression (Supplementary Fig. S10E). Furthermore, a more quantitative me-RIP-qPCR analysis on ALKBH5-silenced osteosarcoma cells and tumor tissues from ALKBH5 KD group showed increased m^{6}A level and decreased expression of RNF40 compared with scrambled group (Supplementary Fig. S10F–S10H). Next, we asked whether like USP22, ALKBH5 KD, and consequently increased m^{6}A levels may affect RNF40 stability. Indeed, ALKBH5 KD significantly reduced the *RNF40* mRNA stability compared with scrambled siRNA-treated cells (Supplementary Fig. S10I).These results suggest that ALKBH5 may interact with RNF40 and USP22 transcripts to regulate m^{6}A levels and consequently their stability. Indeed, RNA IP results showed both USP22 and RNF40 RNA bind to ALKBH5 (Fig. 5C).

Next, we performed rescue experiments to test whether like USP22, changes in m^{6}A levels may also be critical for RNF40 expression. Our results revealed that though there is a trend of RNF40 rescue in METTL3 knockdown, the magnitude of rescue is not significant (Supplementary Fig. S10J). It is likely that presence of residual amount of METTL3 in METTL3 KD samples may be sufficient to compensate for any change in m^{6}A levels following ALKBH5 knockdown. It is also possible that the RNF40 transcripts may have different kinetics for undergoing methylation–demethylation event.

To further understand how changes in m^{6}A levels may regulate USP22 and RNF40 expression, we sought to identify readers that either stabilize or degrade m^{6}A-containing transcripts. The YTHDF family of proteins serves as readers of m^{6}A by either stabilizing or degrading the target transcripts. To identify whether one or more YTHDF proteins may serve as a reader of a methylated *USP22/RNF40* transcripts, we silenced either YTHDF1, 2, or 3 and also performed rescue experiments by silencing both YTHDF1/2/3 and ALKBH5. Only those readers that when silenced significantly altered the levels of USP22 or RNF40 and/or rescued the effect of ALKBH5 silencing were considered to be bona fide readers for USP22 or RNF40. Our results revealed that YTHDF1 and YTHDF3 knockdown significantly increased the level of USP22 and also rescued the effect of ALKBH5 silencing on USP22 expression, while YTHDF3 knockdown significantly increased the level of RNF40 and also rescued the effect of ALKBH5 silencing on RNF40 expression (Supplementary Fig. S11A and S11B). Together, these results suggest that YTHDF1 and YTHDF3 bind and decide the fate of methylated USP22 and RNF40 mRNAs, respectively.

Next, we addressed whether increased H2Aub levels are due to reduced levels of USP22 in ALKBH5-silenced cells. USP22 silencing led to increased H2Aub levels in osteosarcoma cells (Fig. 5D; Supplementary Fig. S11C). Surprisingly, RNF40 silencing also resulted in increased H2Aub levels in osteosarcoma cells along with expected reduction in H2Bub levels (Fig. 5D; Supplementary Fig. S11C). This was an unexpected finding as RNF40 serves as a writer for H2Bub. To address how RNF40 may regulate H2Aub, we performed a meta-analysis using the RNF40 protein interaction data set. We found that RNF40 may interact with DDB1-CUL4A E3 ligase complex that targets H2A monoubiquitination at the site of DNA damage (Supplementary Fig. S11D; Supplementary Table S3; ref. 42). To validate this observation, we performed coimmunoprecipitation using antibodies against CUL4A/DDB1 and RNF40, and showed that indeed, RNF40 interacts with DDB1–CUL4A complex (Fig. 5E; Supplementary Fig. S11E). This is a significant result as RNF40 interaction with CUL4A has not been previously established. We hypothesized that RNF40 may inhibit DDB1-CUL4A E3 ligase activity resulting in inhibition of H2A monoubiquitination. To test that, we first asked whether RNF40 may regulate DDB1 and/or CUL4A expression. RNF40 knockdown did not have any appreciable effect on DDB1 levels (Fig. 5F; Supplementary Fig. S11F). However, surprisingly, RNF40 knockdown led to significantly increased levels of CUL4A (Fig. 5F; Supplementary Fig. S11F). These results suggested that RNF40 may inhibit stability of DDB1-CUL4A E3 ligase complex and consequently affects its activity. To test that, we performed rescue experiment by knocking down DDB1 in RNF40-silenced cells and determining the H2Aub levels. Silencing of DDB1 rescued the effect of RNF40 silencing on H2A monoubiquitination (Supplementary Fig. S11G). Furthermore, expectedly, RNF40 or DDB1 knockdown resulted in decreased levels of H2Bub as DDB1-CUL4A and RNF40 form an E3 ligase complex that is known to promote H2B monoubiquitination (Supplementary Fig. S11G). These results suggest a novel role for RNF40 in regulating histone H2A monoubiquitination.

Regulation of DNA repair events by the ALKBH5–USP22/RNF40 signaling axis

Histone H2A monoubiquitination is linked with gene silencing by repressing transcription initiation or elongation (43, 44). Because several cell-cycle and DNA repair genes were significantly downregulated in ALKBH5 KD cells with no change in their m^6A status, we reasoned that ALKBH5 may affect transcription of these genes by regulating the promoter occupancy of H2A monoubiquitination. To test this idea, we performed ChIP in scrambled and ALKBH5-silenced osteosarcoma cells using antibodies against H2Aub and primers spanning the promoter regions of cell cycle- and DNA repair-associated genes. H2Aub enrichment on target gene promoters was increased in ALKBH5 KD osteosarcoma cells compared with scrambled siRNA–transfected cells (Fig. 5G). To confirm the repressive state of chromatin on target gene promoters, we performed ChIP using antibody against RNA polymerase II and activating histone mark H3K4me3. RNA Pol II and H3K4me3 enrichment was significantly reduced on cell cycle and DNA repair gene promoters in ALKBH5-silenced cells compared with scrambled-siRNA–transfected cells (Supplementary Fig. S11H). Consistent with that, silencing of RNF40 or USP22 silencing resulted in significantly reduced enrichment of H3K4me3 and RNA pol II on target gene promoters (Supplementary Fig. S11I). To further validate these findings, we performed rescue experiments. USP22 or RNF40 overexpression rescued the effect of ALKBH5

silencing on target gene expression (Supplementary Fig. S12A), and H2Aub-K19 as well as H3K4me3 recruitment to the target gene promoters (Supplementary Fig. S12B and S12C). These results suggest that ALKBH5-USP22/RNF40 signaling may support cell-cycle progression and DNA repair events by inhibiting monoubiquitination of histone H2A and therefore inducing the expression of key replication and DNA repair–associated genes in cancers. Further supporting that, using ISce-I–based DSB repair reporter assays, we show that silencing of USP22 or RNF40 decreased both NHEJ- and HR-mediated DSB repair in osteosarcoma cells (Fig. 5H and I).

USP22 and RNF40 mediate tumor-promoting function of ALKBH5

USP22 is known to have tumor-promoting function, while RNF40 can have both tumor suppressor and oncogenic function in different tumor types (20, 37, 45, 46). We sought to determine the relative roles of USP22 and RNF40 in osteosarcoma. Silencing of either USP22 or RNF40 reduced short-term cell viability and clonogenic growth of osteosarcoma cells (Fig. 6A and B). We performed rescue experiments to test whether ALKBH5's tumor-promoting function may be mediated by USP22 and RNF40. Overexpression of USP22 or RNF40 in ALKBH5 KD osteosarcoma cells partially rescued viability and clonogenic growth, suggesting that USP22 and RNF40 are important effectors by which ALKBH5 imparts its tumor-promoting function (Fig. 6C–E; Supplementary Fig. S12D–S12G). Consistent with that, like ALKBH5, expression of USP22 and RNF40 was higher in osteosarcoma cells lines compared with normal control cells (hFOB and IMR90 for USP22 and IMR90 for RNF40; Supplementary Fig. S13A).

Next, we asked whether ALKBH5 regulation of USP22 and RNF40 is unique to osteosarcoma or it is also present in other cancers. ALKBH5 silencing reduced USP22 and RNF40 expression in breast cancer (MDA-MB-468) and glioblastoma (T98G) cells (Supplementary Fig. S13B–S12D). Furthermore, ALKBH5 knockdown led to increased H2Aub levels in these cancer cell lines (Supplementary Fig. S13E and S13F). Although we saw significant effect of ALKBH5 silencing on USP22 and RNF40 levels in multiple cancer types, we cannot exclude the possibility that ALKBH5-USP22/RNF40 signaling axis may not be similarly active in a specific cancer subtype. Supporting that, we saw a subtle effect of ALKBH5 knockdown on USP22 in MDA-MB-231 cells (Supplementary Fig. S13B). Nevertheless, given that ALKBH5 has protumorigenic role in many cancers (15, 28, 32), our results suggest that ALKBH5-USP22/RNF40 signaling may play an important role in promoting growth and progression of multiple tumors. Further supporting that, gene expression data analyses revealed a strong correlation between ALKBH5 and USP22/RNF40 expression in multiple cancer types (Fig. 6F; Supplementary Fig. S13G–S13I). Taken together, these results suggest that m^6A modification has a critical role in tumor growth and progression by affecting the epigenetic state of key genes that regulate cell-cycle and DNA repair events in cancer cells (Fig. 6G).

Discussion

There has not been any significant advancement in the treatment outcome for patients with osteosarcoma in last three decades. This is in part because no targetable recurrent mutations

have been identified. In this study, we show that RNA demethylase ALKBH5 is uniquely amplified and has a protumorigenic function in osteosarcomas. Although it is not clear how ALKBH5 may be amplified specifically in osteosarcoma, we propose that the amplification event may be an outcome of chromatid breakage fusion bridge cycle as osteosarcoma has rather chaotic genome as evidenced by the recurrent chromosomal rearrangements. Our study shows that ALKBH5 controls histone ubiquitination and downstream DNA-based events to regulate osteosarcoma growth and progression. We demonstrate that ALKBH5 regulates USP22 and RNF40 expression and subsequently alters histone ubiquitination to activate cell cycle and DNA repair genes in osteosarcoma. Furthermore, we show that increased expression and activity of ALKBH5 plays a causal role in USP22/RNF40 dysregulation and consequently histone ubiquitination in multiple cancers.

These results, along with previous reports (6) showing no apparent defects except for compromised fertility in ALKBH5 knockout mice, indicate that cancer cells may be addicted to ALKBH5. Thus, reduced ALKBH5 activity and levels are deleterious for osteosarcoma cells, whereas ALKBH5's function (such as DNA repair) in normal cells may be compensated by other redundant mechanisms. For example, ALKBH5 may support a specific alternative DNA repair pathway that cancer cells depend on to survive and proliferate, while normal cells are equipped with many DNA repair mechanisms to cope with loss of ALKBH5. One such alternative DNA repair pathway that cancer cells get addicted to is alternative nonhomologous end joining (alt-NHEJ). Alt-NHEJ serves as the backup mechanism for repairing DNA (albeit at the cost of genomic stability) caused by stalled replication forks. Several proteins including PARP1 and PolB that promote alt-NHEJ are highly expressed in cancers including osteosarcoma. Moreover, PolB-overexpressing mice have been reported to have increased incidence of osteosarcoma (47). Furthermore, ALKBH5 target USP22 is shown to be critical for optimal alternative end-joining-mediated DNA repair (48). In addition, it is possible that replication and cell cycle–associated genes (e.g., MCMs, CDC6, and cyclin B1) that are overexpressed in cancers may be more sensitive to changes in ALKBH5 and m^6A levels than normal cells (49, 50). These observations suggest that ALKBH5 could be a potent therapeutic target in cancer in general and osteosarcoma in particular, because it appears that inhibiting ALKBH5 activity could have potent antitumor effects without serious toxicities.

Histone tails undergo extensive post-translational modifications that together regulate several key cellular processes by impacting the chromatin structure and controlling transcriptional activity. An example of one such modification is the monoubiquitination of lysines on histone H2A and H2B tails. H2B ubiquitination is reported to promote di- and tri-methylation of H3K4 and H3K79, and may assist in transcriptional regulation. On the other hand, H2A (the most abundant ubiquitinated protein in the nucleus of mammalian cells) is associated with gene silencing and X-chromosome inactivation (51, 52). Histone monoubiquitination is tightly controlled, because its dysregulation is frequently associated with cancer (53). Bmi1, Ring1B, and USP22, all involved in regulation of histone ubiquitination or deubiquitination, were among the 11 genes identified as "death from cancer" signature genes, which predict poor prognosis in multiple cancers (29). In addition, RNF40 is highly expressed in cancers and may play critical role in regulating cancer cell

proliferation (24, 26). Despite their critical role in tumorigenesis, how histone ubiquitination is regulated in cancers remains unclear.

Here, we show that the m^6A RNA methylation plays a critical role in regulating histone ubiquitination events in cancers. We show that increased levels and activity of the RNA demethylase ALKBH5 induces histone deubiquitinase USP22 and E3 ubiquitin ligase RNF40 expression to support cancer cell proliferation and progression. Our results reveal that silencing of ALKBH5 led to a significant increase in H2Aub, but not H2Bub. Because levels of the ubiquitin ligases RING1A/RING1B, which act in concert to add an ubiquitin moiety to H2A were unchanged, reducing levels of deubiquitinases (such as ubiquitin-specific proteases 22) results in increased steady-state levels of H2Aub in ALKBH5-silenced cancer cells. Previous reports showed decreased global H2Aub levels in cancers (54). Furthermore, the USPs that target H2A (USP22, USP21, and USP16) are reported to act as oncogenes (41, 55). Moreover, we did not see compensatory increase in the expression of other USPs (USP3, USP21, and USP16) that can deubiquitinate H2Aub (41, 55), rather we saw decreased expression of USP16, suggesting that these USPs may not compensate for the loss of USP22 in ALKBH5-silenced cancer cells. In addition, our results suggest that RNF40 contributes to increased H2Aub in ALKBH5-silenced cancer cells. Supporting that, we show that RNF40 interacts with DDB1-CUL4A ligase complex that targets H2A mono-ubiquitination in response to DNA damage (56, 57). Our results suggest that RNF40 inhibits H2A monoubiquitination by binding and affecting the stability of DDB1-CUL4A ubiquitin ligase complex, while reduced levels of RNF40 (as in ALKBH5-silenced cancer cells) stabilize DDB1-CUL4A E3 ligase complex to ubiquitinate H2A, resulting in transcriptional suppression of target genes. Because RNF40 interacts with DDB1-CUL4A E3 ligase complex that promotes H2B monoubiquitination, our results suggest that RNF40–DDB1–CUL4A interaction may favor H2B monoubiquitination at the expense of H2A monoubiquitination.

However, unlike H2A, unchanged H2Bub levels in ALKBH5-silenced cells suggest that decreased levels of RNF40—which acts as the writer for H2Bub—may compensate for the loss of USP22-which also acts as the eraser for H2Bub. In addition, other deubiquitinases (such as USP36, USP42, USP43, USP44, USP49, or USP51) that act as erasers of H2Bub mark may compensate for the loss of USP22 in ALKBH5-silenced cells. However, a study by Atanassov and colleagues showed that USP22 knockdown may not increase the global H2Bub levels in some cells. This will suggest that other writers/erasers of ubiquitination may play a role in regulating H2Bub levels in ALKBH5-silenced cancer cells. Although, we did not see changes in H2Bub level, it is possible that specific genomic loci may exhibit altered H2Bub levels due to alteration in RNF40 and USP22 expression, which may also contribute to ALKBH5 function.

Our results reveal that ALKBH5 regulates DNA repair in osteosarcoma cells. Depletion of ALKBH5 in the presence and absence of ionizing radiation resulted in increased γH2AX levels and 53BP1 foci. Furthermore, using functional studies, we demonstrate that ALKBH5 and its target genes USP22 and RNF40 inhibit H2A ubiquitination and promote the expression of DNA repair genes in osteosarcoma cells. It is likely that changes in USP22 and RNF40 status due to altered levels of m^6A may direct the DNA repair machinery to

employ or not employ HR or NHEJ to repair damaged DNA. In line with that concept, UV radiation induces H2A ubiquitination at H2AK119 (58). Furthermore, our results show that inhibition of DDB-1-CUL4A ligase activity rescued the effect of RNF40 silencing on DNA repair protein in osteosarcoma cells. Moreover, USP22 promotes both HR (23) and NHEJ (48, 59). Since ubiquitination of distinct sites on H2A affects different DNA damage response (60), we cannot exclude the possibility that m^6A may also regulate other ubiquitin ligases and deubiquitinases in addition to USP22 and RNF40 to repair damaged DNA. Furthermore, USP22 can regulate DNA repair events by targeting the deubiquitination of proteins other than H2A (22, 23, 37, 45), it is possible that in addition to H2Aub, other USP22 target proteins may contribute to ALKBH5's DNA repair and oncogenic functions. Example of such targets could be MMP9 and MTA1, which we found to be reduced in ALKBH5-silenced osteosarcoma cells and are reported to be regulated by USP22 (18, 61). Moreover, both MMP9 and MTA1 have well documented roles in tumor progression, and are highly expressed in osteosarcoma (62, 63). These observations, together with our results showing induction of checkpoint proteins in ALKBH5-silenced cancer cells, suggest that maintaining steady-state levels of m^6A is critical for deubiquitination of damaged loci and consequently deactivation of checkpoints, leading to transcriptional reactivation of critical genes that control growth and proliferation of cancer cells.

In addition to H2Aub, RNF40-mediated H2Bub is known to play critical roles in DNA repair (23, 64). Our studies showing no change in H2Bub; increased H2Aub; and reduced HR and NHEJ-mediated DNA repair in RNF40-silenced cancer cells, suggest that RNF40 may also regulate DNA repair process in H2Aub-dependent manner. Consistent with that, we show that RNF40 interacts with DDB1-CUL4A complex, which is reported to maintain genomic integrity by regulating DNA repair processes (42). Our results showing involvement of both USP22 and RNF40-DDB1-CUL4A in regulating H2Aub and DNA repair events suggest that USP22 and RNF40 may functionally interact. Supporting that notion, USP22 is known to deubiquitinate nucleotide excision repair protein XPC (37). Notably, DDB1-CUL4A ubiquitin ligase complex, which we show to interact with RNF40, ubiquitinates XPC during damage.

In summary, there are several key observations in this study. First, our study suggests that m^6A RNA methylation is critical for maintaining an optimal ratio of histone deubiquitinase and ubiquitin ligase to control H2A ubiquitination. Second, we demonstrate a previously undefined mechanism by which expression of histone deubiquitinase USP22 and ubiquitin ligase RNF40 is regulated in cancers. This finding is significant because regulation of histone ubiquitination in cancers is poorly understood. Furthermore, uncovering the mechanisms that leads to overexpression of USP22 in cancer will elucidate its function and may inform approaches to target its oncogenic role. Third, our study is first to show a role for RNF40-DDB1-CUL4A in regulating H2AK119 ubiquitination. Finally, our results support the notion that hyperactive ALKBH5 sets up an aberrant epigenetic program to support cancers. Therefore, approached aimed at targeting ALKBH5 will have immense translational potential to treat cancers, which are dependent on ALKBH5 oncogenic signaling.

Supplementary Material

Refer to Web version on PubMed Central for supplementary material.

Acknowledgments

The authors thank UTHSCSA Genome Sequencing and GCCRI Bioinformatics core facilities for performing RNA sequencing and bioinformatics analysis, respectively. They thank Dr. Suyun Huang (M.D. Anderson Cancer Center, Houston, TX) for lentiviral vector-expressing nontargeting pLKO.1 control shRNA and shRNA targeting ALKBH5. The authors thank Dr. Greg Auni at UTHSCSA for IMR-90 cell line. They thank Dr. Maria Jasin and Dr. Jeremy Stark for DR-GFP integrated U2OS cells and the pCAGGS vector with I-SceI/GFP. They thank Teng Zhang for helping with me-RIP-seq analysis. The authors thank Karen P. Klein (Clarus Editorial Services; https://www.claruseditorialservices.com/) for editing. M.K. Rao is supported by NIH (NCI) grants R01CA179120-01A1 and R01CA239227-A1. M.K. Rao and Y. Gupta are supported by CPRIT grant RP200110. Y. Chen is supported by CPRIT Core Grant RP16073. Y. Chen and M.K. Rao are supported by NCI P30 grant CA054174. P. Houghton is supported by NCI grant CA165995. S. Timilsina is supported by Institutional National Research Service Award (NRSA), NCI T32 CA148724. P. Yadav is supported by CPRIT training grant RP170345.

Authors' Disclosures

Y.K. Gupta reports non-financial support from Atomic Therapeutics outside the submitted work. No disclosures were reported by the other authors.

References

1. Mirabello L, Troisi RJ, Savage SA. International osteosarcoma incidence patterns in children and adolescents, middle ages and elderly persons. Int J Cancer 2009; 125:229–34. [PubMed: 19330840]
2. Kansara M, Teng MW, Smyth MJ, Thomas DM. Translational biology of osteosarcoma. Nat Rev Cancer 2014;14:722–35. [PubMed: 25319867]
3. Wu B, Li L, Huang Y, Ma J, Min J. Readers, writers and erasers of N(6)-methylated adenosine modification. Curr Opin Struct Biol 2017;47:67–76. [PubMed: 28624569]
4. Ping X-L, Sun B-F, Wang L, Xiao W, Yang X, Wang W-J, et al. Mammalian WTAP is a regulatory subunit of the RNA N6-methyladenosine methyltransferase. Cell Res 2014;24:177–89. [PubMed: 24407421]
5. Jia G, Fu Y, Zhao X, Dai Q, Zheng G, Yang Y, et al. N6-methyladenosine in nuclear RNA is a major substrate of the obesity-associated FTO. Nat Chem Biol 2011;7:885–7. [PubMed: 22002720]
6. Zheng G, Dahl JA, Niu Y, Fedorcsak P, Huang C-M, Li CJ, et al. ALKBH5 is a mammalian RNA demethylase that impacts RNA metabolism and mouse fertility. Mol Cell 2013;49:18–29. [PubMed: 23177736]
7. Li A, Chen Y-S, Ping X-L, Yang X, Xiao W, Yang Y, et al. Cytoplasmic m(6)A reader YTHDF3 promotes mRNA translation. Cell Res 2017;27:444–7. [PubMed: 28106076]
8. Wang X, Zhao BS, Roundtree IA, Lu Z, Han D, Ma H, et al. N(6)-methyladenosine modulates messenger RNA translation efficiency. Cell 2015;161:1388–99. [PubMed: 26046440]
9. Batista PJ, Molinie B, Wang J, Qu K, Zhang J, Li L, et al. m(6)A RNA modification controls cell fate transition in mammalian embryonic stem cells. Cell Stem Cell 2014;15:707–19. [PubMed: 25456834]
10. Fustin J-M, Doi M, Yamaguchi Y, Hida H, Nishimura S, Yoshida M, et al. RNA-methylation-dependent RNA processing controls the speed of the circadian clock. Cell 2013;155:793–806. [PubMed: 24209618]
11. Han D, Liu J, Chen C, Dong L, Liu Y, Chang R, et al. Anti-tumour immunity controlled through mRNA m(6)A methylation and YTHDF1 in dendritic cells. Nature 2019;566:270–4. [PubMed: 30728504]
12. Barbieri I, Tzelepis K, Pandolfini L, Shi J, Millán-Zambrano G, Robson SC, et al. Promoter-bound METTL3 maintains myeloid leukaemia by m(6)A-dependent translation control. Nature 2017;552:126–31. [PubMed: 29186125]

13. Miao W, Chen J, Jia L, Ma J, Song D. The m6A methyltransferase METTL3 promotes osteosarcoma progression by regulating the m6A level of LEF1. Biochem Biophys Res Commun 2019;516:719–25. [PubMed: 31253399]
14. Ling Z, Chen L, Zhao J. m6A-dependent up-regulation of DRG1 by METTL3 and ELAVL1 promotes growth, migration, and colony formation in osteosarcoma. Biosci Rep 2020;40:BSR20200282.
15. Zhang C, Samanta D, Lu H, Bullen JW, Zhang H, Chen I, et al. Hypoxia induces the breast cancer stem cell phenotype by HIF-dependent and ALKBH5-mediated m(6)A-demethylation of NANOG mRNA. Proc Natl Acad Sci U S A 2016; 113:E2047–56. [PubMed: 27001847]
16. Yuan Y, Yan G, He M, Lei H, Li L, Wang Y, et al. ALKBH5 suppresses tumor progression via an m(6)A-dependent epigenetic silencing of pre-miR-181b-1/YAP signaling axis in osteosarcoma. Cell Death Dis 2021;12:60. [PubMed: 33431791]
17. Chen S, Zhou L, Wang Y. ALKBH5-mediated m(6)A demethylation of lncRNA PVT1 plays an oncogenic role in osteosarcoma. Cancer Cell Int 2020;20:34. [PubMed: 32021563]
18. Zhang X-Y, Varthi M, Sykes SM, Phillips C, Warzecha C, Zhu W, et al. The putative cancer stem cell marker USP22 is a subunit of the human SAGA complex required for activated transcription and cell-cycle progression. Mol Cell 2008;29:102–11. [PubMed: 18206973]
19. Shiloh Y, Shema E, Moyal L, Oren M. RNF20-RNF40: A ubiquitin-driven link between gene expression and the DNA damage response. FEBS Lett 2011;585: 2795–802. [PubMed: 21827756]
20. Melo-Cardenas J, Zhang Y, Zhang DD, Fang D. Ubiquitin-specific peptidase 22 functions and its involvement in disease. Oncotarget 2016;7:44848–56. [PubMed: 27057639]
21. Lin Z, Tan C, Qiu Q, Kong S, Yang H, Zhao F, et al. Ubiquitin-specific protease 22 is a deubiquitinase of CCNB1. Cell Discov 2015;1:15028. [PubMed: 27030811]
22. Gennaro VJ, Stanek TJ, Peck AR, Sun Y, Wang F, Qie S, et al. Control of CCND1 ubiquitylation by the catalytic SAGA subunit USP22 is essential for cell cycle progression through G1 in cancer cells. Proc Natl Acad Sci U S A 2018;115: E9298–307. [PubMed: 30224477]
23. Nardi IK, Stark JM, Larsen A, Salgia R, Raz DJ. USP22 interacts with PALB2 and promotes chemotherapy resistance via homologous recombination of DNA double-strand breaks. Mol Cancer Res 2020;18:424–35. [PubMed: 31685642]
24. Jääskeläinen T, Makkonen H, Visakorpi T, Kim J, Roeder RG, Palvimo JJ. Histone H2B ubiquitin ligases RNF20 and RNF40 in androgen signaling and prostate cancer cell growth. Mol Cell Endocrinol 2012;350:87–98. [PubMed: 22155569]
25. Tarcic O, Granit RZ, Pateras IS, Masury H, Maly B, Zwang Y, et al. RNF20 and histone H2B ubiquitylation exert opposing effects in Basal-Like versus luminal breast cancer. Cell Death Differ 2017;24:694–704. [PubMed: 28157208]
26. Zheng X, Chen K, Liu X, Pan Y, Liu H. High RNF40 expression indicates poor prognosis of hepatocellular carcinoma. Int J Clin Exp Pathol 2018;11:2901–6. [PubMed: 31938414]
27. Imam JS, Plyler JR, Bansal H, Prajapati S, Bansal S, Rebeles J, et al. Genomic loss of tumor suppressor miRNA-204 promotes cancer cell migration and invasion by activating AKT/mTOR/Rac1 signaling and actin reorganization. PLoS One 2012;7:e52397. [PubMed: 23285024]
28. Zhang S, Zhao BS, Zhou A, Lin K, Zheng S, Lu Z, et al. m(6)A demethylase ALKBH5 maintains tumorigenicity of glioblastoma stem-like cells by sustaining FOXM1 expression and cell proliferation program. Cancer Cell 2017;31: 591–606. [PubMed: 28344040]
29. Glinsky GV, Berezovska O, Glinskii AB. Microarray analysis identifies a death-from-cancer signature predicting therapy failure in patients with multiple types of cancer. J Clin Invest 2005;115:1503–21. [PubMed: 15931389]
30. Cui X, Zhang L, Meng J, Rao MK, Chen Y, Huang Y. MeTDiff: a novel differential RNA methylation analysis for MeRIP-seq data. IEEE/ACM Trans Comput Biol Bioinform 2018;15:526–34. [PubMed: 29610101]
31. Cui X, Wei Z, Zhang L, Liu H, Sun L, Zhang S-W, et al. Guitar: an R/Bioconductor package for gene annotation guided transcriptomic analysis of RNA-related genomic features. Biomed Res Int 2016;2016:8367534. [PubMed: 27239475]

32. Panneerdoss S, Eedunuri VK, Yadav P, Timilsina S, Rajamanickam S, Viswanadhapalli S, et al. Cross-talk among writers, readers, and erasers of m(6)A regulates cancer growth and progression. Sci Adv 2018;4: eaar8263. [PubMed: 30306128]
33. Meng J, Cui X, Rao MK, Chen Y, Huang Y. Exome-based analysis for RNA epigenome sequencing data. Bioinformatics 2013;29:1565–7. [PubMed: 23589649]
34. Shen L, Liang Z, Yu H. Dot blot analysis of N6-methyladenosine RNA modification levels. Bio Protoc 2017;7:e2095.
35. Yang J, Li Q, Noureen N, Fang Y, Kurmasheva R, Houghton PJ, et al. PCAT: an integrated portal for genomic and preclinical testing data of pediatric cancer patient-derived xenograft models. Nucleic Acids Res 2021;49: D1321–7. [PubMed: 32810235]
36. Knudsen KE, Booth D, Naderi S, Sever-Chroneos Z, Fribourg AF, Hunton IC, et al. RB-dependent S-phase response to DNA damage. Mol Cell Biol 2000;20: 7751–63. [PubMed: 11003670]
37. Mccann JJ, Vasilevskaya IA, Poudel Neupane N, Shafi AA, Mcnair C, Dylgjeri E, et al. USP22 functions as an oncogenic driver in prostate cancer by regulating cell proliferation and DNA repair. Cancer Res 2020;80:430–43. [PubMed: 31740444]
38. Wang X, Lu Z, Gomez A, Hon GC, Yue Y, Han D, et al. N6-methyladenosine-dependent regulation of messenger RNA stability. Nature 2014;505:117–20. [PubMed: 24284625]
39. Schwartz S, Mumbach MR, Jovanovic M, Wang T, Maciag K, Bushkin GG, et al. Perturbation of m6A writers reveals two distinct classes of mRNA methylation at internal and 5' sites. Cell Rep 2014;8:284–96. [PubMed: 24981863]
40. Zhang X-Y, Pfeiffer H, Thorne A, Mcmahon SB. USP22, an hSAGA subunit and potential cancer stem cell marker, reverses the polycomb-catalyzed ubiquitylation of histone H2A. Cell Cycle 2008;7:1522–4. [PubMed: 18469533]
41. Cao J, Yan Q. Histone ubiquitination and deubiquitination in transcription, DNA damage response, and cancer. Front Oncol 2012;2:26. [PubMed: 22649782]
42. Lovejoy CA, Lock K, Yenamandra A, Cortez D. DDB1 maintains genome integrity through regulation of Cdt1. Mol Cell Biol 2006;26:7977–90. [PubMed: 16940174]
43. Tamburri S, Lavarone E, Fernández-Pérez D, Conway E, Zanotti M, Manganaro D, et al. Histone H2AK119 mono-ubiquitination is essential for polycomb-mediated transcriptional repression. Mol Cell 2020;77:840–56. [PubMed: 31883952]
44. Zhou W, Zhu P, Wang J, Pascual G, Ohgi KA, Lozach J, et al. Histone H2A monoubiquitination represses transcription by inhibiting RNA polymerase II transcriptional elongation. Mol Cell 2008;29:69–80. [PubMed: 18206970]
45. Kim D, Hong A, Park HI, Shin WH, Yoo L, Jeon SJ, et al. Deubiquitinating enzyme USP22 positively regulates c-Myc stability and tumorigenic activity in mammalian and breast cancer cells. J Cell Physiol 2017;232: 3664–76. [PubMed: 28160502]
46. Yang X, Zang H, Luo Y, Wu J, Fang Z, Zhu W, et al. High expression of USP22 predicts poor prognosis and advanced clinicopathological features in solid tumors: a meta-analysis. Onco Targets Ther 2018;11:3035–46. [PubMed: 29872315]
47. Lange SS, Takata K-I, Wood RD. DNA polymerases and cancer. Nat Rev Cancer 2011;11:96–110. [PubMed: 21258395]
48. Ramachandran S, Haddad D, Li C, Le MX, Ling AK, So CC, et al. The SAGA deubiquitination module promotes DNA repair and class switch recombination through ATM and DNAPK-mediated gammaH2AX formation. Cell Rep 2016; 15:1554–65. [PubMed: 27160905]
49. Lim N, Townsend PA. Cdc6 as a novel target in cancer: Oncogenic potential, senescence and subcellular localisation. Int J Cancer 2020;147:1528–34. [PubMed: 32010971]
50. Hassan KA, Ang KK, El-Naggar AK, Story MD, Lee JI, Liu D, et al. Cyclin B1 overexpression and resistance to radiotherapy in head and neck squamous cell carcinoma. Cancer Res 2002;62:6414–7. [PubMed: 12438226]
51. Meas R, Mao P. Histone ubiquitylation and its roles in transcription and DNA damage response. DNA Repair 2015;36:36–42. [PubMed: 26422137]
52. Zhou W, Wang X, Rosenfeld MG. Histone H2A ubiquitination in transcriptional regulation and DNA damage repair. Int J Biochem Cell Biol 2009;41: 12–5. [PubMed: 18929679]

53. Duan Y, Huo D, Gao J, Wu H, Ye Z, Liu Z, et al. Ubiquitin ligase RNF20/40 facilitates spindle assembly and promotes breast carcinogenesis through stabilizing motor protein Eg5. Nat Commun 2016;7:12648. [PubMed: 27557628]
54. Zhu P, Zhou W, Wang J, Puc J, Ohgi KA, Erdjument-Bromage H, et al. A histone H2A deubiquitinase complex coordinating histone acetylation and H1 dissociation in transcriptional regulation. Mol Cell 2007;27: 609–21. [PubMed: 17707232]
55. Citterio E Fine-tuning the ubiquitin code at DNA double-strand breaks: deubiquitinating enzymes at work. Front Genet 2015;6:282. [PubMed: 26442100]
56. Guerrero-Santoro J, Kapetanaki MG, Hsieh CL, Gorbachinsky I, Levine AS, Rapić-Otrin V. The cullin 4B-based UV-damaged DNA-binding protein ligase binds to UV-damaged chromatin and ubiquitinates histone H2A. Cancer Res 2008;68:5014–22. [PubMed: 18593899]
57. G. Kapetanaki M, Guerrero-Santoro J, Bisi DC, Hsieh CL, Rapić-Otrin V, Levine AS. The DDB1-CUL4ADDB2 ubiquitin ligase is deficient in xeroderma pigmentosum group E and targets histone H2A at UV-damaged DNA sites. Proc Natl Acad Sci U S A 2006;103:2588–93. [PubMed: 16473935]
58. Bergink S, Salomons FA, Hoogstraten D, Groothuis TAM, De Waard H, Wu J, et al. DNA damage triggers nucleotide excision repair-dependent monoubiquitylation of histone H2A. Genes Dev 2006;20:1343–52. [PubMed: 16702407]
59. Li C, Irrazabal T, So CC, Berru M, Du L, Lam E, et al. The H2B deubiquitinase Usp22 promotes antibody class switch recombination by facilitating nonhomologous end joining. Nat Commun 2018;9:1006. [PubMed: 29520062]
60. Uckelmann M, Sixma TK. Histone ubiquitination in the DNA damage response. DNA Repair 2017;56:92–101. [PubMed: 28624371]
61. Ning Z, Wang A, Liang J, Xie Y, Liu J, Yan Q, et al. USP22 promotes epithelialmesenchymal transition via the FAK pathway in pancreatic cancer cells. Oncol Rep 2014;32:1451–8. [PubMed: 25070659]
62. Kunz P, Sähr H, Lehner B, Fischer C, Seebach E, Fellenberg J. Elevated ratio of MMP2/MMP9 activity is associated with poor response to chemotherapy in osteosarcoma. BMC Cancer 2016;16:223. [PubMed: 26979530]
63. Kim SS, Park Y-K. Significance of MTA1 in the molecular characterization of osteosarcoma. Cancer Metastasis Rev 2014;33:981–91. [PubMed: 25315817]
64. So CC, Ramachandran S, Martin A. E3 Ubiquitin ligases RNF20 and RNF40 are required for Double-Stranded Break (DSB) repair: Evidence for monoubiquitination of histone H2B lysine 120 as a novel axis of DSB signaling and repair. Mol Cell Biol 2019;39:e00488–18. [PubMed: 30692271]

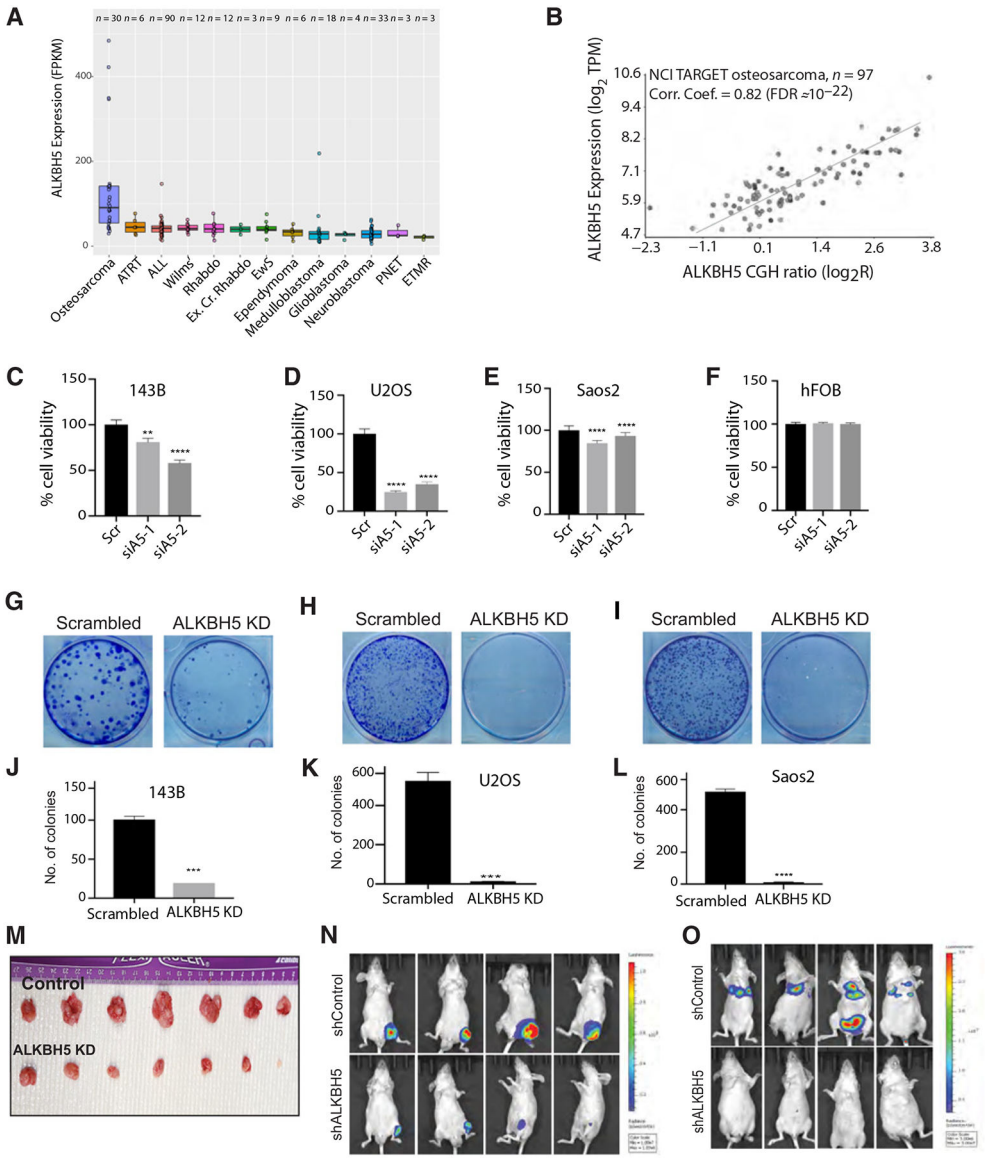

Figure 1.

RNA demethylase ALKBH5 is amplified in osteosarcoma and promotes growth and progression of osteosarcoma. **A**, Pan-cancer analysis using pediatric preclinical testing consortium dataset showing expression of *ALKBH5* gene in patient-derived xenografts. The data was generated using PCAT (35). **B**, Comparative genomic hybridization and RNA-seq data from TARGET database showing amplification of the *ALKBH5* gene and strong correlations between ALKBH5 expression and copy number changes in osteosarcoma samples. **C–F**, Percent of cell viability (measured by CellTiter-Glo luminescent or Alamar Blue cell viability assays) in scrambled siRNA (Scr), ALKBH5 siRNA-1 (siA5–1), or ALKBH5 siRNA-2 (siA5–2)–transfected 143B (**C**), U2OS (**D**), Saos2 (**E**), and hFOB cells (**F**). **G–I**, Clonogenic assays of 143B (**G**), U2OS (**H**), and Saos2 (**I**) cells transfected with scrambled siRNA or ALKBH5 siRNA (ALKBH5 KD). **J–L**, Bar graphs showing mean number of crystal violet–stained colonies counted from **Fig. 1G–I. M**, Photographs showing

representative tumor growth in nude mice injected with 1×10^6 143B cells stably expressing shControl ($n = 7$) or shALKBH5 ($n = 7$). **N**, Photographs showing representative tumor growth in mice intratibially implanted with 143B cells stably transfected with control (shControl; $n = 5$) or ALKBH5 shRNA (shALKBH5; n 5). **O**, Photographs showing representative metastatic lesion in mice intravenously injected with 143B cells stably transfected with control (shControl; $n = 5$) or ALKBH5 shRNA (shALKBH5; $n = 5$). Data shown in **C–F** and **J–L** are means ± SEM ($n \geq 3$ independent experiments). For **C–F**, P values were calculated using one-way ANOVA followed by Dunnett multiple comparison test. **, $P < 0.01$; ***, $P < 0.001$; ****, $P < 0.0001$.

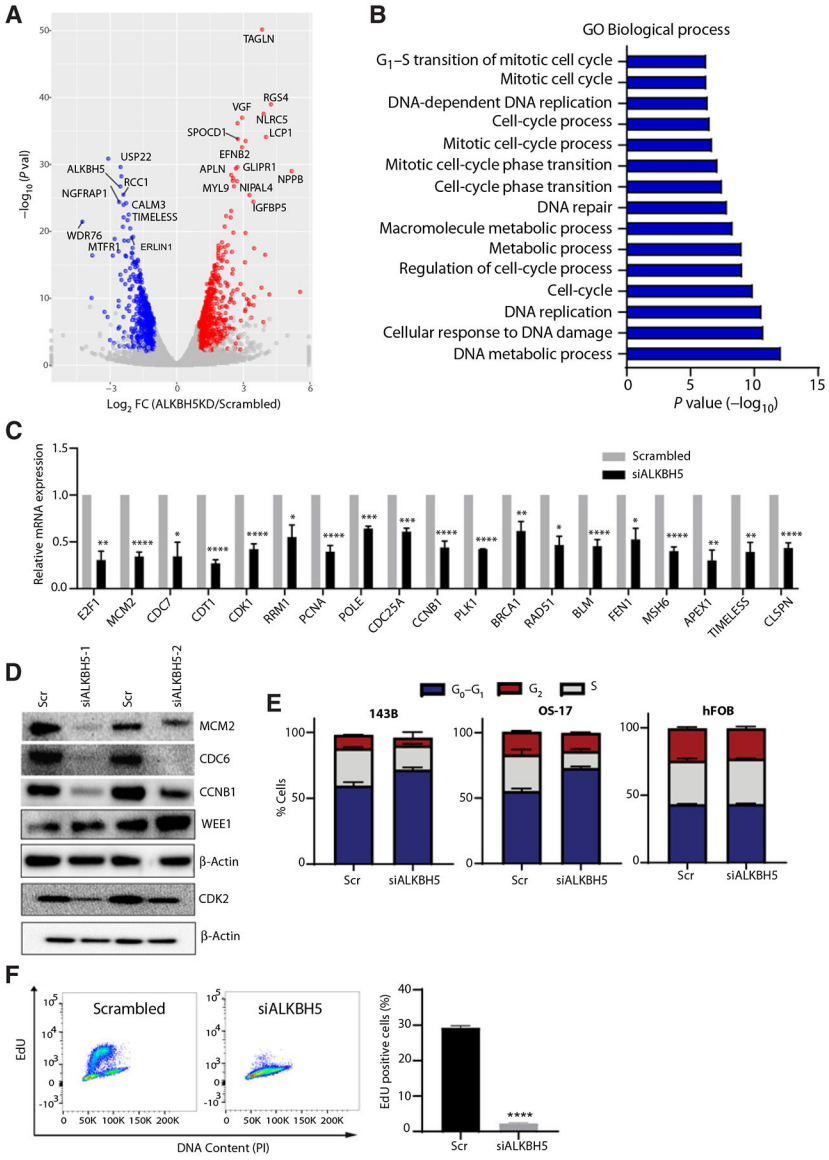

Figure 2.

ALKBH5 promotes cell-cycle progression by regulating cell cycle and DNA replication–associated gene expression. **A**, Volcano plot showing gene expression changes in 143B cells transfected with scrambled siRNA or siALKBH5 (KD) for 48 hours. Cut-off criteria for differentially expressed genes include absolute $\log_2$-fold change >1 and *P* value < 0.05 (red, differentially increased; blue, decreased genes). **B**, Results of gene ontology (GO) analysis showing highly enriched biological processes in ALKBH5 KD 143B cells (reduced genes). **C**, Results of qRT-PCR analysis of target gene expression in 143B cells transfected with scrambled or ALKBH5 siRNA-1 (siALKBH5). **D**, Western blots of target genes in scrambled and two different siRNAs against ALKBH5 (siALKBH5–1 and siALKBH5–2)-transfected 143B cells using antibodies against the indicated proteins. β-Actin was used as the loading control. Gel photograph is representative of at least three independent experiments. The Western blots showing MCM2, CDC6, CCNB1, WEE1, and β-actin were

run on one gel (after stripping), while CDK2 and β-actin were run on a separate gel. **E**, Cell-cycle distribution of 143B, OS-17, or hFOB cells transfected with scrambled or ALKBH5 siRNA. Propidium Iodide was used to stain for DNA content and flow cytometry analysis was done to identify cell population in different phases of cell cycle using FlowJo software. **F**, Bivariate cell-cycle analysis of EdU immunofluorescence versus DNA content of U2OS cells pulse labeled with EdU. Bar graph shows quantification of EdU^+ cells in scrambled and ALKBH5 siRNA–transfected U2OS cells. *P* values calculated using standard Student *t* tests. *, $P < 0.05$; **, $P < 0.01$; ***, $P < 0.001$; ****, $P < 0.0001$. Bar graphs represent means ± SEM for at least three independent experiments.

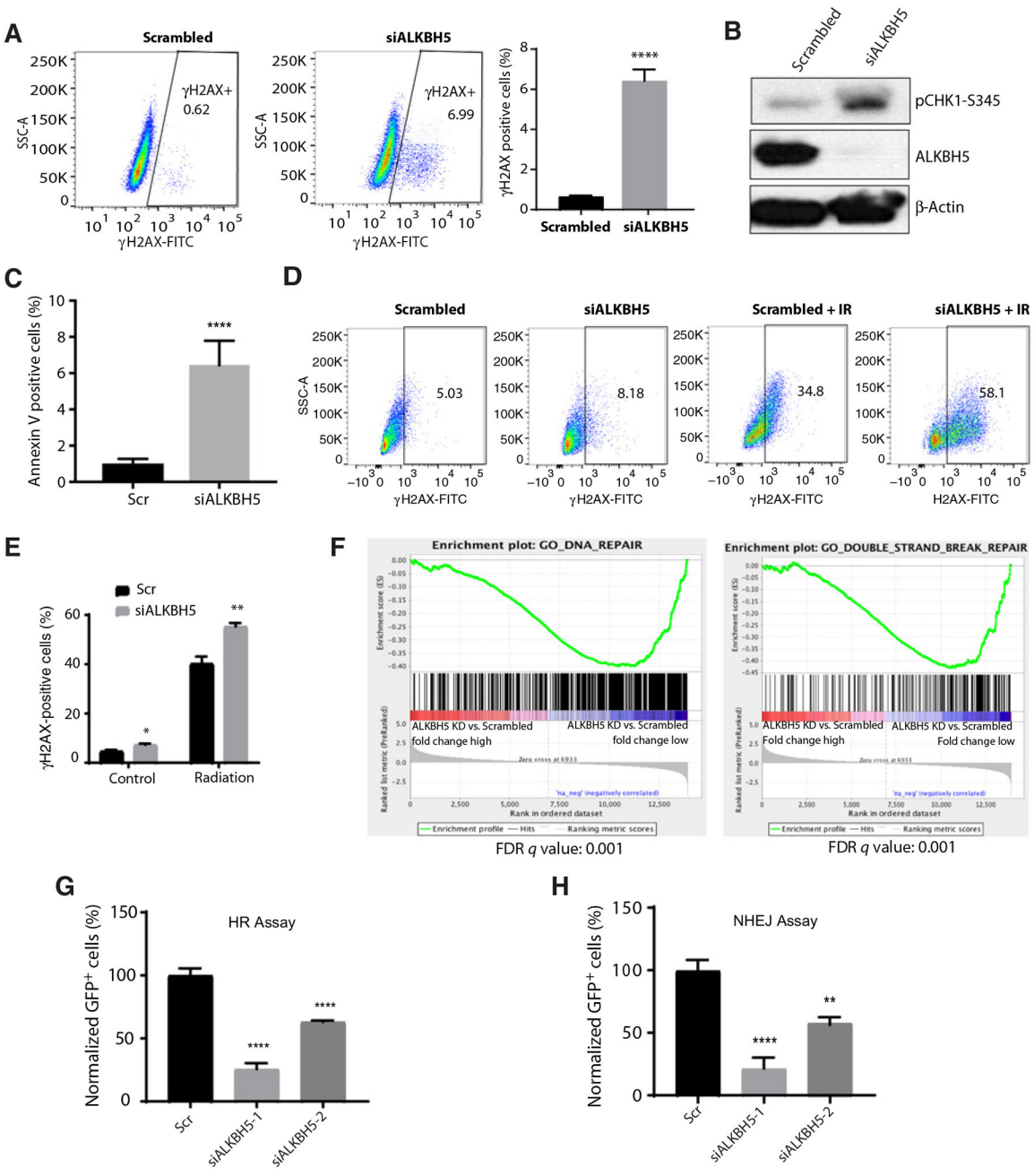

Figure 3.

ALKBH5 regulates DNA damage repair events in cancer cells. **A**, Representative dot plots showing γH2AX-positive cells in scrambled siRNA or ALKBH5 siRNA–transfected U2OS cells. U2OS cells were transfected with scrambled siRNA or ALKBH5 siRNA for 72 hours before flow cytometry analyses. Bar graph shows means ± SEM ($n = 3$). **B**, Western blots of scrambled and ALKBH5 siRNA–transfected U2OS cells using antibodies against the indicated proteins. β-Actin was used as the loading control. **C**, Percent of Annexin V-FITC–positive U2OS cells transfected with scrambled or ALKBH5 siRNA. **D**, Results of flow cytometry showing γH2AX-positive cells in scrambled siRNA and ALKBH5 siRNA–

transfected 143B osteosarcoma cells. Cells were treated with no ionizing radiation (IR) or 10 Gy IR. After 24 hours, cells were stained for γH2AX to estimate unrepaired double-strand breaks. **E**, Bar graphs show quantification of γH2AX-positive cells shown in **D**. *P* values for **A**, **C**, and **E** were calculated using standard Student *t* tests. Bar graph represents means ± SEM ($n = 3$). **F**, GSEA showing enrichment of DNA damage repair pathway in ALKBH5 KD cells compared with scrambled siRNA–transfected 143B cells. **G**, Results of DR-GFP reporter assay showing DSB-induced HR repair. U2OS-DR-GFP cells were transfected with scrambled siRNA or ALKBH5 siRNAs followed by transfection with a pCAGGS vector expressing I-SceI endonuclease or empty vector as control. I-SceI endonuclease expression induces DSB if repaired by HR results in GFP^+ cells as determined by flow cytometry analysis. **H**, EJ5-GFP reporter assay showing total NHEJ. EJ5-GFP U2OS cells were transfected with scrambled siRNA or ALKBH5 siRNAs followed by transfection with a pCAGGS vector expressing I-SceI endonuclease or empty vector as control. I-SceI endonuclease induced DSB if repaired by NHEJ results in GFP^+ cells as determined by flow cytometry. For **G** and **H**, bar graphs show means ± SEM ($n = 3$). *P* values were calculated using one-way ANOVA followed by Dunnett multiple comparisons test. *, $P < 0.05$ **, $P < 0.01$; ****, $P < 0.0001$.

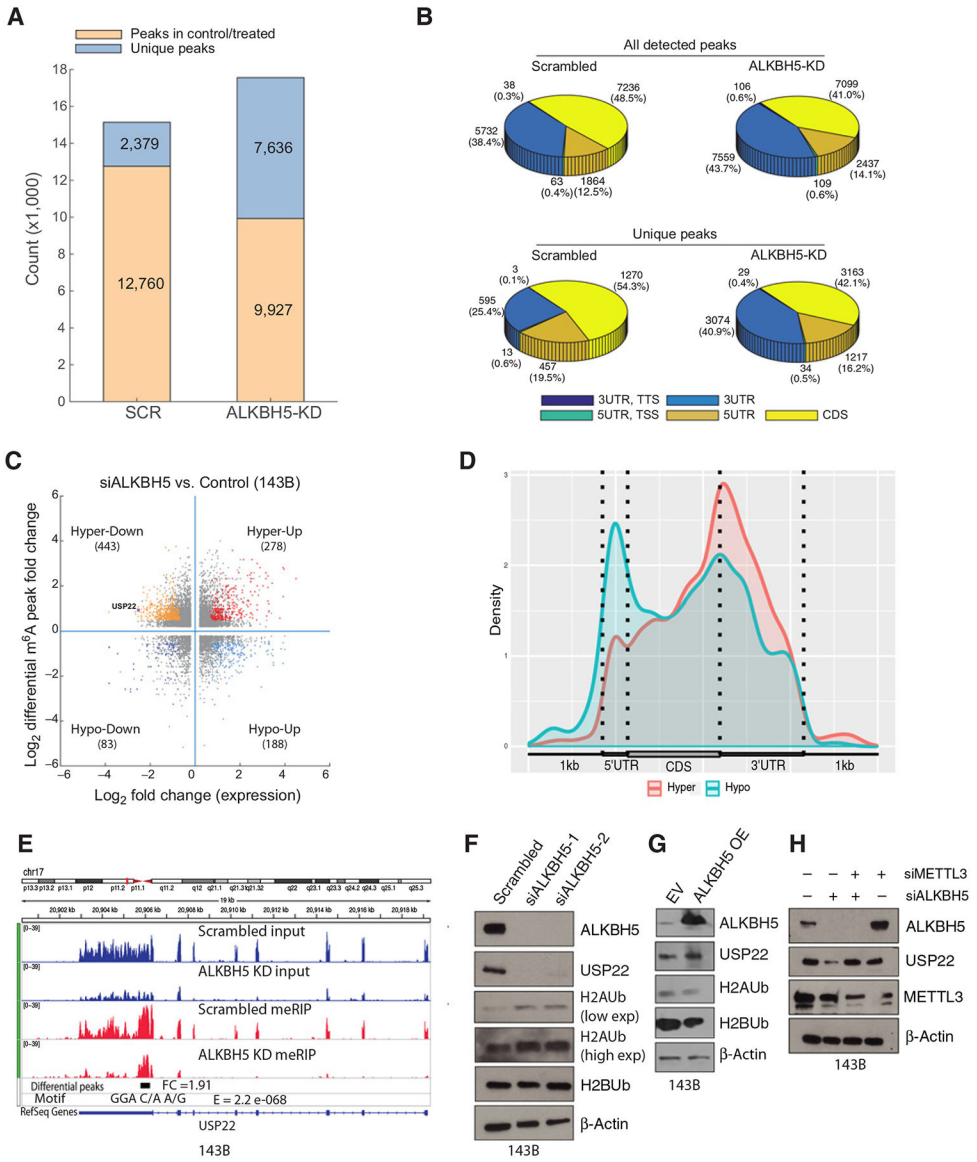

Figure 4.

m^{6}A methylation analyses of control and ALKBH5-silenced OS cells. **A**, Number of peaks identified in scrambled siRNA (SCR) and ALKBH5 siRNA (ALKBH5 KD)–transfected 143B cells using me-RIP-seq. Common m^{6}A-containing genes share at least one common peak, while unique m^{6}A-containing genes share no peak between scrambled siRNA and ALKBH5 KD OS cells. **B**, Proportion of total (top) and unique (bottom) m^{6}A peaks in different regions of genes in scrambled siRNA and ALKBH5 siRNA (ALKBH5 KD)–transfected 143B cells. **C**, Distribution analysis of genes with significant changes in both m^{6}A and expression levels in ALKBH5 knockdown 143B cells compared with scrambled siRNA–transfected cells. **D**, Distribution of hyper and hypo m^{6}A peaks in different regions of mRNA. **E**, USP22 shows significantly enriched m^{6}A peaks (adj $P < 0.05$) in ALKBH5 siRNA or scrambled siRNA–transfected 143B cells. Top two tracks (blue) represent input and bottom two represent me-RIP results for scrambled siRNA and ALKBH5 siRNA–

transfected 143B cells, respectively. Detected differential m^6A peak sites and its fold-change values (differential peak track) were calculated by dividing total m^6A value by expression level of the target site for the specific gene using MeTDiff program. m^6A motif (shown as motif GGA C/A A/G) distribution was determined by subjecting me-RIP-seq data to MEME-ChIP (E value = 2.2 e-068). **F**, Western blots of target genes in scrambled siRNA and ALKBH5 siRNA–transfected 143B OS cells using antibodies against the indicated proteins. β-Actin was used as loading control. **G**, Western blots of target genes in empty vector or ALKBH5 expression plasmid–transfected 143B cells using antibodies against the indicated proteins. β-Actin was used as the loading control. **H**, Western blots of target genes in scrambled siRNA, ALKBH5 siRNA, METTL3 siRNA, or ALKBH5+ METTL3 siRNA–transfected 143B cells using antibodies against the indicated proteins. β-Actin was used as the loading control. Gel photographs are representative of at least three independent experiments.

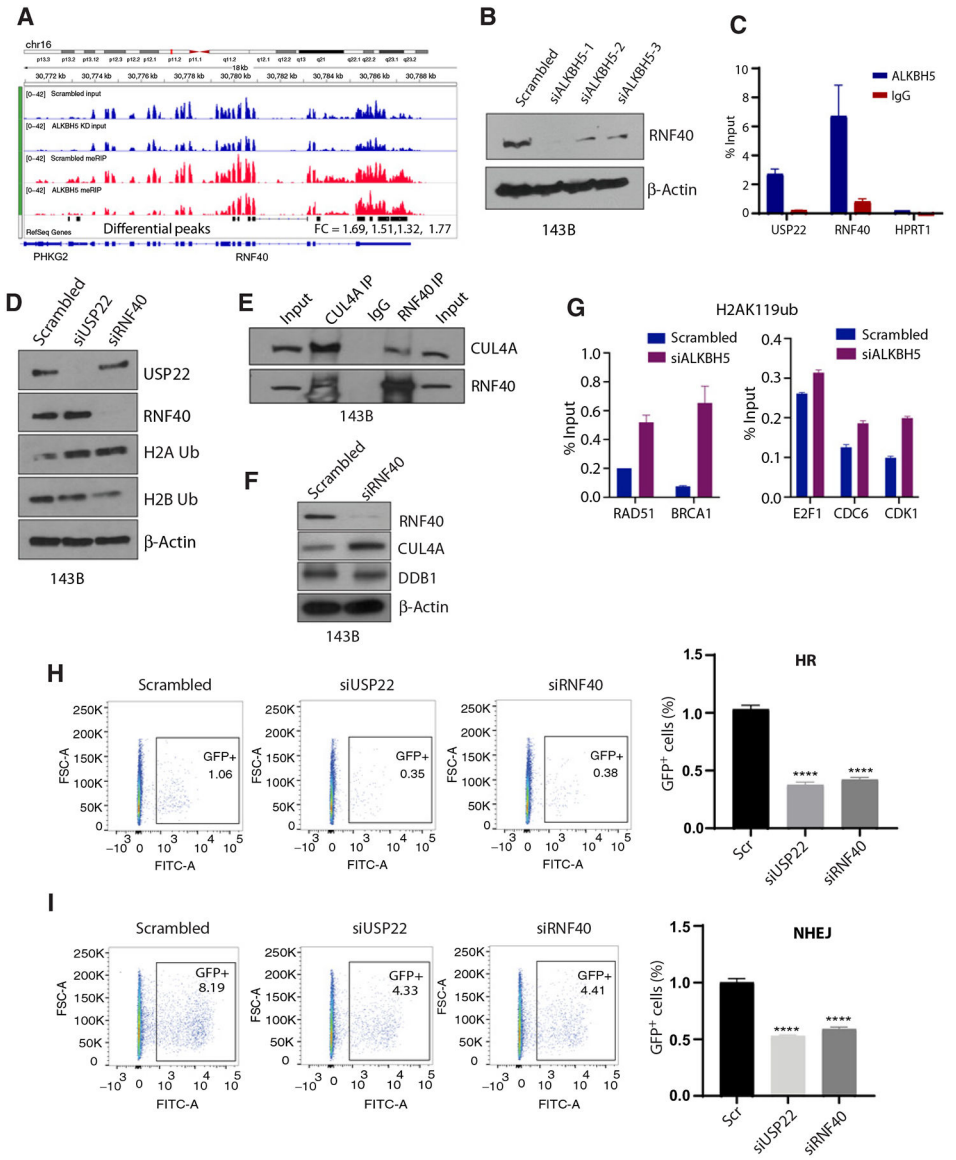

Figure 5.

ALKBH5-USP22/RNF40 axis regulates histone H2AK119 monoubiquitination and DNA damage repair. **A**, RNF40 has significantly enriched m^{6}A peaks (adj $P < 0.05$) in ALKBH5 siRNA–transfected 143B cells compared with scrambled siRNA–transfected cells. Top two tracks (blue) represent input and bottom two show MeRIP results for scrambled siRNA and ALKBH5 siRNA–transfected 143B cells, respectively. Detected differential m^{6}A peak sites and its fold-change values (differential peak track) were calculated by dividing total m^{6}A value by expression level of the target site for the specific gene using MeTDiff program. **B**, Western blots analysis of scrambled siRNA and ALKBH5 siRNA–transfected 143B cells using antibody against RNF40. β-Actin was used as a loading control. **C**, qRT- PCR results showing enrichment of ALKBH5 target genes *USP22* and *RNF40* in 143B cells after RNA immunoprecipitation using antibodies against ALKBH5 or IgG. HPRT1 was the negative control. **D**, Western blots showing RNF40 and USP22 as well as and monoubiquitinated

H2A (H2A ub) and H2B (H2B ub) levels in scrambled, USP22-siRNA, or RNF40-siRNA–transfected 143B cells using antibodies against the indicated proteins. β-Actin was used as the loading control. **E**, Immunoprecipitation assay with RNF40, CUL4A, or IgG antibody using 143B lysate. Immunoblotting is shown for RNF40 and CUL4A. **F**, Western blot showing RNF40, CUL4A, and DDB1 levels in scrambled or RNF40-siRNA–transfected 143B cells. β-Actin was used as a loading control. Gel picture is representative of at least three independent experiments. **G**, qRT-PCR results in 143B cells transfected with scrambled siRNA or ALKBH5 siRNA subjected to ChIP using antibodies against H2Aub K119. Bar graphs show histone mark enrichment near the promoter region of genes shown in the graph. Data displayed as percentages of input and error bars represent ± SEM of technical triplicates. **H**, FACS analysis showing GFP positive cells from DR-GFP assay reflecting DSB-induced HR repair. U2OS-DR-GFP cells were transfected with scrambled siRNA, USP22-siRNA (siUSP22), or RNF40-siRNA (siRNF40), followed by transfection with a pCAGGS vector expressing I-SceI endonuclease or empty vector as control. **I**, FACS showing GFP-positive cells from EJ5-GFP reporter assay reflecting total NHEJ. EJ5-GFP U2OS cells were transfected with scrambled siRNA, USP22 siRNA (siUSP22), or RNF40 siRNA (siRNF40), followed by transfection with pCAGGS vector expressing I-SceI endonuclease or empty vector as control. *P* values for **H** and **I** were calculated using one-way ANOVA followed by Dunnett multiple comparisons test. Bar graph shows means ± SEM ($n = 3$). ****, $P < 0.0001$.

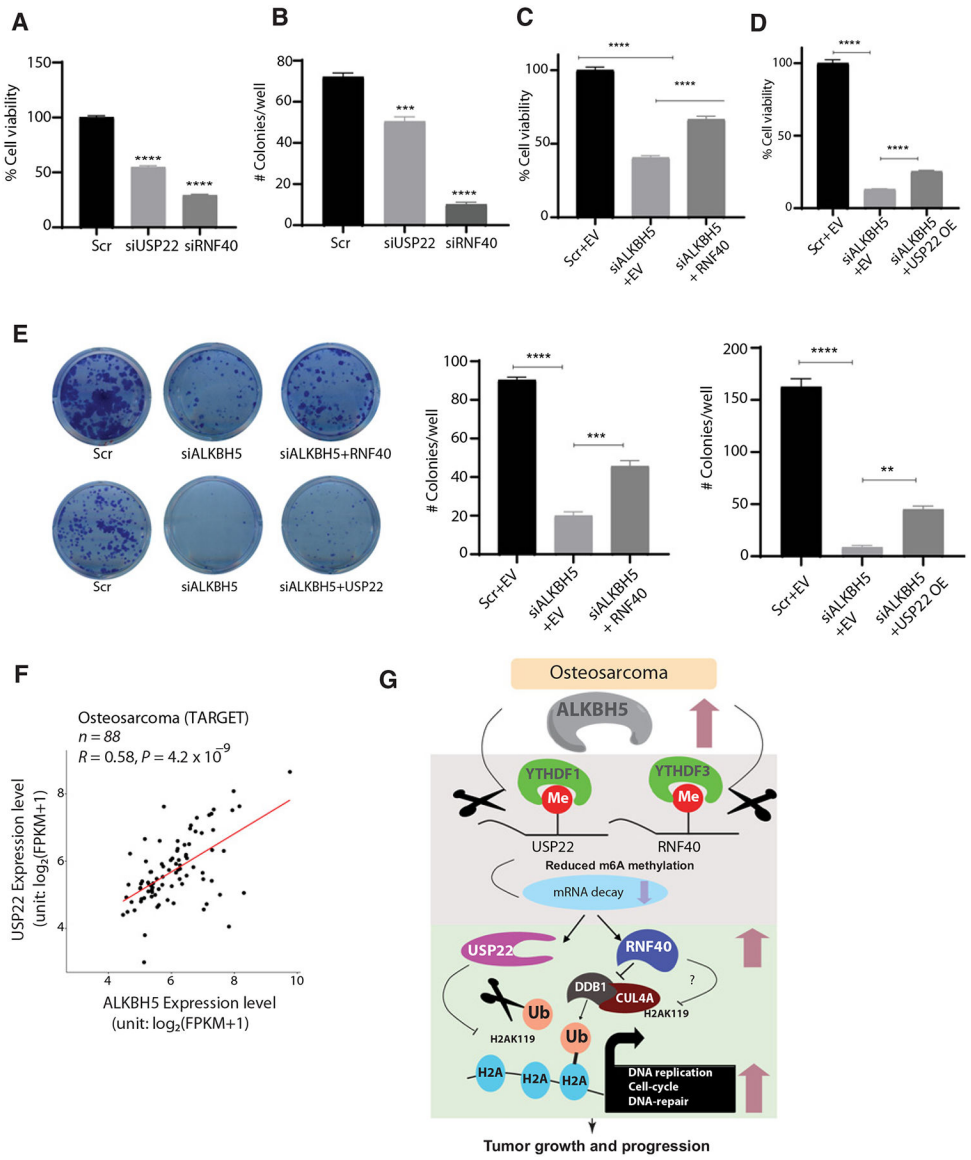

Figure 6.

USP22 and RNF40 mediate protumorigenic effects of ALKBH5 ALKBH5-USP22/RNF40 axis to regulate histone H2AK119 monoubiquitination and DNA damage repair. **A**, Bar graph showing percentage cell viability in scrambled siRNA (Scr), USP22-siRNA (siUSP22), or RNF40-siRNA (siRNF40)–transfected 143B cells. Cell viability was measured by CellTiter-Glo luminescent cell viability assay. **B**, Clonogenic assay of 143B cells transfected with scrambled siRNA, USP22 siRNA, or RNF40 siRNA. Bar graph shows number of crystal violet–stained colonies counted per well. **C** and **D**, Bar graphs showing percentage cell viability of 143B cells cotransfected with scrambled siRNA + empty vector (EV) or ALKBH5 siRNA + EV or ALKBH5 siRNA + RNF40 overexpression plasmid (**C**); Scr + empty vector (EV) or ALKBH5 siRNA + EV or ALKBH5 siRNA + USP22 overexpression plasmid (**D**). **E**, Results of clonogenic assays of 143B cells cotransfected with scrambled siRNA + EV or ALKBH5 siRNA + EV or ALKBH5

siRNA + USP22 or RNF40 overexpression plasmid. Bar graph shows means ± SEM of crystal violet–stained colonies counted per well. **F**, Osteosarcoma tumor samples from the TARGET database show significant correlations between ALKBH5 and USP22 expression. **A–E**, Bar graphs show mean SEM ($n = 3$). P values calculated using one-way ANOVA followed by Dunnett multiple comparisons test. **, $P < 0.01$; ***, $P < 0.001$; ****, $P < 0.0001$. **G**, Model showing mechanism by which ALKBH5 promotes osteosarcoma growth and progression. Our results suggest that amplification of ALKBH5 resulting in its overexpression leads to decreased m^6A methylation and consequently increased stability of histone deubiquitinase USP22 and ubiquitin ligase RNF40 in osteosarcoma. The increased stability of USP22 in turn results in increased deubiquitination and reduced levels of monoubiquitinated histone H2A. On the other hand, the increased stability of RNF40 in ALKBH5 overexpressing osteosarcoma leads to increased interaction and inhibition of DDB1-CUL4A ligase complex resulting in reduced levels of monoubiquitinated histone H2A. The reduction in monoubiquitinated histone H2A, which compacts chromatin and acts as a transcriptional repressive mark, transactivates key progrowth/tumorigenic genes, causing unchecked cell-cycle progression, continuous replication, and DNA repair to support osteosarcoma growth.